AIMS Mathematics, 11(4): 10311–10341.
DOI: 10.3934/math.2026426
Received: 17 January 2026
Revised: 31 March 2026
Accepted: 08 April 2026
Published: 15 April 2026

https://www.aimspress.com/journal/Math

Research article

A novel Bernstein operational matrix approach for tempered fractional differential equations: Convergence and stability analysis

Jalal Al Hallak[1,2,*], Mohammed Alshbool[2], Ishak Hashim[1], Eddie Shahril Ismail[1] and Shaher Momani[3,4]

[1] Department of Mathematical Sciences, Universiti Kebangsaan Malaysia, Bangi, 43600, Selangor, Malaysia
[2] Department of Mathematics and Statistics, Zayed University, Abu Dhabi, United Arab Emirates
[3] Nonlinear Dynamics Research Center (NDRC), Ajman University, Ajman, P.O. Box 346, United Arab Emirates
[4] Department of Mathematics, Faculty of Science, University of Jordan, Amman, 11942, Jordan

* **Correspondence:** Email: Jalal.Alhallak@zu.ac.ae.

Abstract: Tempered fractional differential equations (TFDEs) incorporate exponential decay into fractional operators to account for truncated memory and semi-long-range dependence in a variety of applications, including anomalous diffusion, viscoelasticity, transport phenomena, geophysical processes, and financial dynamics. In this work, a tempered fractional Bernstein method (TFBM) was proposed for the numerical solution of TFDEs involving Caputo-type derivatives. The proposed formulation combined a Bernstein polynomial approximation with an analytic representation of the Caputo–tempered fractional derivative through operational matrices. On this basis, two collocation-based variants were developed, namely, a Chebyshev-type method (TFBM-C) and a Legendre-type method (TFBM-L). For the linear setting, a convergence analysis established norm convergence of the numerical solution to the exact solution as the polynomial degree increased under standard stability and consistency assumptions. Stability was investigated under perturbations in the forcing term as well as under combined perturbations in the system matrix and righthand side, and explicit norm-wise error bounds were derived using classical matrix perturbation theory. Numerical experiments involving linear and nonlinear TFDEs, weakly singular solutions, multi-term operators, and benchmark test problems demonstrated that the proposed methods achieve higher accuracy than finite-difference and shifted Legendre operational matrix schemes while maintaining low computational cost.

Keywords: tempered fractional differential equations; Bernstein operational matrices; Caputo fractional derivative; convergence analysis; stability analysis; error estimate
Mathematics Subject Classification: 65L05, 26A33

1. Introduction

The mathematical idea of differentiation of non-integer order is not a modern development. It can be traced back to the late seventeenth century, following a well-known exchange between Leibniz and L'Hôpital concerning the interpretation of derivatives of arbitrary order. What initially appeared as a theoretical curiosity gradually evolved into a structured mathematical framework through the later contributions of Euler, Liouville, and Fourier. These developments ultimately led to several widely adopted definitions, including the Riemann–Liouville, Caputo, Riesz, and Hilfer derivatives, which now form the basis of many fractional modeling approaches. Such operators are particularly well suited for describing systems where nonlocal interactions and memory effects play a dominant role [1].

Over the past decades, fractional differential equations (FDEs) have been successfully applied to model a variety of anomalous phenomena that cannot be adequately captured by classical integer-order models. In economic applications, fractional formulations have been used to represent long-memory effects in growth models and financial dynamics [2]. In physics and engineering, they naturally arise in the study of anomalous diffusion and transport processes in heterogeneous or fractal media [3]. Fractional models have also found applications in epidemiology and chaos theory, where memory-dependent mechanisms and complex temporal interactions are essential for an accurate description of the underlying dynamics [4–6]. More recently, extensions such as fuzzy fractional calculus have been introduced to address uncertainty and imprecision in data-driven systems [7]. In parallel, the growing interaction between fractional calculus and machine learning has motivated hybrid frameworks, including neural networks guided by variable-order fractional operators [8].

Significant advances have also been achieved in the theoretical study of Caputo fractional derivatives in more complex settings. For example, higher-order integrodifferential inclusions of Volterra–Fredholm type with impulses and infinite delay have been investigated, and rigorous existence results have been established [9]. In a related line of work, the approximate controllability of impulsive fractional differential equations of order $1 < r < 2$ with infinite delay has been analyzed using functional analytic techniques [10]. Taken together, these results demonstrate the ability of Caputo-based models to represent complex nonlocal dynamics with memory effects.

Despite their flexibility, classical fractional operators based on power-law kernels are not always well suited for practical modeling. In particular, the assumption of infinite memory and the resulting unbounded variance may be incompatible with physical systems evolving over finite spatial or temporal domains. Tempered fractional calculus (TFC) was proposed to alleviate these issues by introducing an exponential tempering factor into the kernel. This modification effectively weakens long-range memory effects while preserving the essential fractional character of the model. As a consequence, tempered formulations exhibit finite variance and allow for a smooth transition between anomalous and classical diffusion, which is especially relevant for describing transient anomalous diffusion observed in geophysical and hydrological applications [11, 12].

Tempered fractional differential equations (TFDEs) therefore provide a practical and mathematically consistent framework for modeling nonlocal processes with controlled memory decay. Their applicability has been demonstrated in a wide range of problems, including turbulent and non-Gaussian transport in fluid dynamics [11], subdiffusive flow in porous and groundwater systems [13], hereditary transport phenomena in biophysical media such as blood flow and viscoelastic materials [12], and thermal conduction models [14]. From a theoretical viewpoint, TFDEs have been

formulated using tempered Caputo, tempered Riemann–Liouville, and substantial derivatives, and their well-posedness has been rigorously investigated under various boundary and terminal conditions [15, 16]. As a result, TFDEs have become a central topic in modern fractional calculus, attracting sustained interest in their theory [17], numerical treatment [18, 19], and practical applications [20–22].

The nonlocal nature of tempered fractional operators poses substantial challenges for numerical computation. A wide range of numerical techniques has been proposed to address TFDEs, including finite difference schemes for Riesz-tempered and multi-term time-fractional models [16,23], predictor–corrector algorithms and their fast variants for tempered Caputo equations [24, 25], and spectral methods based on Chebyshev, Jacobi, and Laguerre polynomials, which can achieve high accuracy for smooth solutions [12, 14]. Additional approaches include sinc-collocation methods for problems on unbounded domains [26], operational matrix techniques for nonlinear and multi-term TFDEs [27], and transform-based methods that yield semi-analytical solutions for specific classes of equations [28, 29]. Nevertheless, these methods often face limitations related to reduced accuracy near weak singularities, high computational cost for long-time simulations, or conditioning issues in the resulting algebraic systems [16, 26, 30].

Efficient and accurate numerical solvers for tempered fractional models continue to attract considerable attention, given their importance in applications such as diffusion, viscoelasticity, and transport phenomena. Among the available approaches, operational matrix methods constructed from suitable basis functions provide a promising alternative, as they can achieve high-order accuracy while keeping the algebraic complexity manageable. In particular, Bernstein-based operational matrix techniques have recently gained interest as effective numerical tools for fractional and nonlinear problems, owing to their ability to handle weak singularities and to preserve good numerical conditioning [31–33].

Motivated by these advances, this paper introduces the tempered fractional Bernstein method (TFBM) for the numerical solution of a broad class of tempered fractional differential equations. The central contribution of the proposed method is a formulation in which two distinct sources of numerical error are controlled independently: The polynomial approximation error, governed by the Bernstein degree n, and the truncation error associated with the analytic series representation of the Caputo–tempered derivative, controlled by a separate parameter M. Unlike existing Bernstein-based fractional or tempered fractional schemes, this explicit decoupling allows the accuracy of the solution representation and the fractional operator to be tuned independently. The proposed framework also naturally accommodates both Chebyshev–Gauss and Legendre–Gauss collocation strategies within a unified Bernstein–tempered setting.

A key limitation of many existing numerical methods for tempered fractional differential equations lies in the difficulty of controlling different sources of numerical error independently, together with potential conditioning issues and a loss of accuracy in the presence of weak singularities. The proposed TFBM complements and extends existing approaches in several directions. Variational and finite element methods for tempered operators, such as the Galerkin formulation of Deng and Zhang [13] and the well-posedness analysis of Zaky [16], provide a rigorous framework; however, they typically rely on mesh refinement, which can increase computational cost. By comparison, TFBM attains spectral-type accuracy without requiring a mesh. Efficient history compression techniques for time-fractional and tempered equations, including fast convolution and sum-of-exponentials methods [25], significantly reduce memory usage and computational cost in long-time simulations.

These approaches, however, mainly address temporal nonlocality and can be naturally combined with TFBM. Spectral and operational matrix methods based on orthogonal polynomials [14, 27, 45] achieve high-order accuracy for smooth solutions, but may encounter conditioning issues or reduced efficiency when fractional power singularities are present. In contrast, the fractional Bernstein basis allows the transformation ($x = \tau^{\delta}$), which facilitates the treatment of such features and leads, in practice, to well-conditioned collocation systems.

The fractional Bernstein basis is particularly well suited to tempered fractional problems, since this transformation provides a natural representation of fractional-type behavior near the initial point while preserving good numerical conditioning and compatibility with the operational matrix formulation. Physics-informed neural networks (PINNs), such as the Monte Carlo-based approach of Hu et al. [34], offer considerable flexibility for high-dimensional and inverse problems, but rely on stochastic training procedures and still lack a comprehensive convergence theory for fractional operators. Taken together, these approaches reflect different trade-offs: mesh-based methods provide geometric flexibility at the cost of higher computational expense, fast convolution techniques reduce temporal complexity, spectral methods deliver high accuracy but may suffer from conditioning issues, and PINNs offer flexibility at the expense of increased computational and theoretical uncertainty. Within this broader setting, TFBM offers a deterministic, mesh-free, and high-accuracy alternative supported by convergence and stability analysis.

This work introduces a TFBM for Caputo–tempered fractional differential equations, based on a Bernstein polynomial representation combined with an operational matrix formulation of the tempered fractional derivative. A distinctive feature of the method is the explicit separation between the polynomial approximation error and the truncation error arising from the series representation of the operator, which makes it possible to control these two sources of error independently. The formulation incorporates both Chebyshev–Gauss and Legendre–Gauss collocation within a unified framework. A rigorous theoretical analysis is then developed to establish the main properties of the method.

The remainder of this paper is organized as follows. Section 2 introduces the necessary preliminaries and definitions from tempered fractional calculus. Section 3 presents the formulation of the proposed tempered fractional Bernstein method. Convergence, stability, and computational complexity analyses are provided in Section 4. Numerical experiments illustrating the accuracy and robustness of the method are reported in Section 5. Finally, Section 6 summarizes the main findings and outlines potential directions for future research.

2. Preliminaries

Throughout this work, we consider left-sided tempered fractional operators on $[\tau_1, \tau_2]$ with order $0 < \delta < 1$ and tempering parameter $\omega \geq 0$. The tempered Riemann–Liouville fractional integral is denoted by $\mathcal{J}_{\tau_1}^{\delta,\omega}$, while the corresponding tempered Riemann–Liouville and Caputo derivatives are denoted by $\mathcal{D}_{\tau_1}^{\delta,\omega}$ and ${}^{C}\mathcal{D}_{\tau_1}^{\delta,\omega}$, respectively, following standard formulations [35–37].

Definition 1. *Let $0 < \delta < 1$, $\omega \geq 0$, and $v \in L^1(\tau_1, \tau_2)$. For $\tau \in (\tau_1, \tau_2]$, the left-sided tempered Riemann–Liouville fractional integral of order δ is defined by*

$$\mathcal{J}_{\tau_1}^{\delta,\omega} v(\tau) := \frac{1}{\Gamma(\delta)} \int_{\tau_1}^{\tau} (\tau - s)^{\delta-1} e^{-\omega(\tau-s)} v(s)\, ds, \tag{2.1}$$

where $\Gamma(\cdot)$ denotes the Euler Gamma function. For $\omega = 0$, this definition reduces to the classical Riemann–Liouville fractional integral

$$\mathcal{J}^{\delta}_{\tau_1} v(\tau) := \frac{1}{\Gamma(\delta)} \int_{\tau_1}^{\tau} (\tau - s)^{\delta-1} v(s)\, ds.$$

Definition 2. *Let $v(\tau) \in C[\tau_1, \tau_2]$, $0 < \delta < 1$, and $\omega \geq 0$. The left-sided tempered Riemann–Liouville fractional derivative of order δ is defined by*

$$\mathcal{D}^{\delta,\omega}_{\tau_1} v(\tau) := \frac{e^{-\omega\tau}}{\Gamma(1-\delta)} \frac{d}{d\tau} \int_{\tau_1}^{\tau} (\tau - s)^{-\delta} e^{\omega s} v(s)\, ds. \tag{2.2}$$

Definition 3. *Let $v \in C^1[\tau_1, \tau_2]$, $0 < \delta < 1$, and $\omega \geq 0$. The left-sided Caputo–tempered fractional derivative of order δ with tempering parameter ω is defined by*

$${}^{C}\mathcal{D}^{\delta,\omega}_{\tau_1} v(\tau) := e^{-\omega\tau}\, {}^{C}\mathcal{D}^{\delta}_{\tau_1}(e^{\omega\tau} v(\tau)), \qquad \tau \in (\tau_1, \tau_2], \tag{2.3}$$

where ${}^{C}\mathcal{D}^{\delta}_{\tau_1}$ denotes the classical Caputo fractional derivative of order δ. This exponential-conjugation formulation is standard in the theory of tempered fractional calculus [35, 36].

For $0 < \delta < 1$, Definition 3 is equivalent to the integral representation

$${}^{C}\mathcal{D}^{\delta,\omega}_{\tau_1} v(\tau) = \frac{e^{-\omega\tau}}{\Gamma(1-\delta)} \int_{\tau_1}^{\tau} (\tau - s)^{-\delta} \frac{d}{ds}(e^{\omega s} v(s))\, ds. \tag{2.4}$$

Without loss of generality, the physical interval $[\tau_1, \tau_2]$ is mapped onto the reference interval $[0, 1]$ via an affine transformation. Henceforth, all operators are expressed on $[0, 1]$. For notational simplicity, we write ${}^{C}\mathcal{D}^{\delta,\omega}_{\tau}$ to denote the left-sided Caputo–tempered derivative with fixed lower terminal 0.

Definition 4. *Let $n \in \mathbb{N}$ and $\mu = 0, 1, \ldots, n$. The classical Bernstein polynomial of degree n on $[0, 1]$ is defined by*

$$\mathcal{B}_{\mu,n}(\tau) := \binom{n}{\mu} \tau^{\mu} (1 - \tau)^{n-\mu}, \qquad \tau \in [0, 1]. \tag{2.5}$$

For $0 < \delta < 1$, the fractional Bernstein basis is defined by

$$\mathcal{B}^{\delta}_{\mu,n}(\tau) := \binom{n}{\mu} \tau^{\mu\delta} (1 - \tau^{\delta})^{n-\mu}, \qquad \tau \in [0, 1]. \tag{2.6}$$

3. TFBM

This section presents a detailed numerical procedure for solving TFDEs using the TFBM. The proposed approach combines Bernstein polynomial approximations with tempered fractional operators to construct an accurate and flexible numerical framework for a wide class of fractional models [37–39].

We consider the Caputo–tempered fractional differential equation of order $0 < \delta < 1$ on the reference interval $[0, 1]$:

$${}^{C}\mathcal{D}^{\delta,\omega}_{\tau} v(\tau) = g(\tau, v(\tau)). \tag{3.1}$$

For $0 < \delta < 1$, a single pointwise condition is prescribed,

$$v(\tau_c) = v_c, \qquad \tau_c \in [0, 1]. \tag{3.2}$$

Here ${}^{C}\mathcal{D}_{\tau}^{\delta,\omega}$ denotes the left-sided Caputo–tempered fractional derivative with tempering parameter $\omega \geq 0$.

The approximate solution is represented in the fractional Bernstein space in the form

$$v_{n,\delta}(\tau) = \sum_{\mu=0}^{n} c_\mu \, \mathcal{B}_{\mu,n}^{\delta}(\tau), \qquad \tau \in [0, 1], \tag{3.3}$$

where the basis functions $\mathcal{B}_{\mu,n}^{\delta}(\tau)$ defined in (2.6) determine the approximation space in which $v_{n,\delta}(\tau)$ is represented. The unknown coefficients $\{c_\mu\}$ are computed using a collocation approach, in which the governing TFDE is enforced at the nodes $\{\tau_j\}_{j=0}^{n-1}$ selected according to Chebyshev–Gauss or Legendre–Gauss distributions on $[0, 1]$, while the prescribed pointwise condition is imposed separately, resulting in an algebraic system for the coefficients.

To numerically approximate the solution of the TFDEs (3.1)–(3.2), we construct an approximate solution using Bernstein polynomial operational matrices as

$$v_{n,\delta}(\tau) = \mathbf{B}_n^{\delta}(\tau)\, \mathbf{C}, \tag{3.4}$$

where

$$\mathbf{B}_n^{\delta}(\tau) = [\mathcal{B}_{0,n}^{\delta}(\tau), \, \mathcal{B}_{1,n}^{\delta}(\tau), \, \cdots, \, \mathcal{B}_{n,n}^{\delta}(\tau)], \qquad \mathbf{C} = \begin{bmatrix} c_0 \\ c_1 \\ \vdots \\ c_n \end{bmatrix}. \tag{3.5}$$

Here, $\mathbf{B}_n^{\delta}(\tau) \in \mathbb{R}^{1\times(n+1)}$ and $\mathbf{C} \in \mathbb{R}^{(n+1)\times 1}$. The functions $\mathcal{B}_{0,n}^{\delta}(\tau), \ldots, \mathcal{B}_{n,n}^{\delta}(\tau)$ are the fractional Bernstein basis functions defined in (2.6), and $c_0, \ldots, c_n$ are unknown coefficients.

$$\mathbf{B}_n^{\delta}(\tau) = \mathbf{T}(\tau)\, \mathbf{Q}^{\top}, \tag{3.6}$$

where the matrices are defined by

$$\mathbf{Q} = \begin{pmatrix} q_{00} & q_{01} & \cdots & q_{0n} \\ q_{10} & q_{11} & \cdots & q_{1n} \\ \vdots & \vdots & \ddots & \vdots \\ q_{n0} & q_{n1} & \cdots & q_{nn} \end{pmatrix}, \qquad \mathbf{T}(\tau) = \begin{bmatrix} 1 & \tau^{\delta} & \tau^{2\delta} & \cdots & \tau^{n\delta} \end{bmatrix}, \tag{3.7}$$

with the entries q_{ij} defined by

$$q_{ij} = \begin{cases} (-1)^{j-i} \binom{n}{i} \binom{n-i}{j-i}, & i \leq j, \\ 0, & i > j. \end{cases} \tag{3.8}$$

Thus, the approximate solution in (3.4) can be written as

$$v_{n,\delta}(\tau) = \mathbf{T}(\tau)\, \mathbf{Q}^{\top} \mathbf{C}. \tag{3.9}$$

For each monomial basis function $\tau^{p\delta}$, $p = 0, 1, \ldots, n$, the left-sided Caputo–tempered fractional derivative of order $\delta \in (0, 1)$ and tempering parameter $\omega \geq 0$ is defined by

$$ {}^{C}\mathcal{D}_{\tau}^{\delta,\omega}\tau^{p\delta} = e^{-\omega\tau}\,{}^{C}\mathcal{D}_{\tau}^{\delta}(e^{\omega\tau}\tau^{p\delta}). \tag{3.10} $$

For $p \geq 1$, expanding the exponential function into its Taylor series and applying the analytic rule for the Caputo fractional derivative of a power function,

$$ {}^{C}\mathcal{D}_{\tau}^{\delta}\tau^{\mu} = \frac{\Gamma(\mu+1)}{\Gamma(\mu+1-\delta)}\,\tau^{\mu-\delta}, $$

yields the exact infinite-series representation

$$ {}^{C}\mathcal{D}_{\tau}^{\delta,\omega}\tau^{p\delta} = e^{-\omega\tau}\sum_{k=0}^{\infty}\frac{\omega^{k}}{k!}\,\frac{\Gamma(k+p\delta+1)}{\Gamma(k+p\delta+1-\delta)}\,\tau^{k+p\delta-\delta}, \qquad p \geq 1. \tag{3.11} $$

Since the summand decays like $k^{\delta}/k!$ and is further attenuated by the factor $e^{-\omega\tau}$, the series can be safely truncated after M terms to obtain the numerical approximation

$$ {}^{C}\mathcal{D}_{\tau,(M)}^{\delta,\omega}\tau^{p\delta} = e^{-\omega\tau}\sum_{k=0}^{M}\frac{\omega^{k}}{k!}\,\frac{\Gamma(k+p\delta+1)}{\Gamma(k+p\delta+1-\delta)}\,\tau^{k+p\delta-\delta}, \qquad p \geq 1. \tag{3.12} $$

Lemma 3.1 (Uniform truncation bound for the tempered Caputo series)**.** *Let $p \geq 1$ be an integer, $\delta \in (0, 1)$, $\omega \geq 0$, and let $M \in \mathbb{N}_0$. Let ${}^{C}\mathcal{D}_{\tau,(M)}^{\delta,\omega}\tau^{p\delta}$ denote the M-term truncation of the series representation of ${}^{C}\mathcal{D}_{\tau}^{\delta,\omega}\tau^{p\delta}$. Then, there exists a constant $C_{p,\delta} > 0$, independent of M, such that*

$$ \sup_{\tau\in[0,1]}\left|{}^{C}\mathcal{D}_{\tau}^{\delta,\omega}\tau^{p\delta} - {}^{C}\mathcal{D}_{\tau,(M)}^{\delta,\omega}\tau^{p\delta}\right| \leq C_{p,\delta}\,e^{\omega}\,\frac{\omega^{M+1}}{M!}. $$

Consequently, the truncation error decays super-algebraically as $M \to \infty$ and is uniform for $\tau \in [0, 1]$.

Proof. From the series representation, the truncation error is

$$ R_{M}(\tau) = e^{-\omega\tau}\sum_{k=M+1}^{\infty}\frac{\omega^{k}}{k!}\,\frac{\Gamma(k+p\delta+1)}{\Gamma(k+p\delta+1-\delta)}\,\tau^{k+p\delta-\delta}. $$

For $\tau \in [0, 1]$ and $p \geq 1$, we have $k + p\delta - \delta = k + (p-1)\delta \geq 1$ and, hence, $|\tau^{k+p\delta-\delta}| \leq 1$. Moreover, $|e^{-\omega\tau}| \leq 1$ for $\omega \geq 0$. Therefore,

$$ |R_{M}(\tau)| \leq \sum_{k=M+1}^{\infty}\frac{\omega^{k}}{k!}\,\frac{\Gamma(k+p\delta+1)}{\Gamma(k+p\delta+1-\delta)}. $$

By Gautschi's inequality [40], for $x > 0$ and $0 < s < 1$,

$$ \frac{\Gamma(x+1)}{\Gamma(x+s)} \leq (x+1)^{1-s}. $$

With $x = k + p\delta$ and $s = 1 - \delta$, we obtain

$$\frac{\Gamma(k + p\delta + 1)}{\Gamma(k + p\delta + 1 - \delta)} \leq (k + p\delta + 1)^{\delta}.$$

Since $p\delta \leq p$ and $k \geq 1$, we have $k + p\delta + 1 \leq k + p + 1 \leq (p + 2)k$, hence

$$(k + p\delta + 1)^{\delta} \leq (p + 2)^{\delta} k^{\delta}.$$

Thus,

$$\frac{\Gamma(k + p\delta + 1)}{\Gamma(k + p\delta + 1 - \delta)} \leq C_{p,\delta}\, k^{\delta}, \qquad C_{p,\delta} = (p + 2)^{\delta}.$$

Because $0 < \delta < 1$, $k^{\delta} \leq k$ for $k \geq 1$, and therefore

$$\frac{k^{\delta}}{k!} \leq \frac{k}{k!} = \frac{1}{(k - 1)!}.$$

Consequently,

$$|R_M(\tau)| \leq C_{p,\delta} \sum_{k=M+1}^{\infty} \frac{\omega^k}{(k - 1)!} = C_{p,\delta}\, \omega \sum_{j=M}^{\infty} \frac{\omega^j}{j!}.$$

Using the standard bound for the tail of the exponential series (see, e.g., [41]),

$$\sum_{j=M}^{\infty} \frac{\omega^j}{j!} \leq e^{\omega} \frac{\omega^M}{M!}, \qquad \omega \geq 0,$$

we obtain

$$|R_M(\tau)| \leq C_{p,\delta}\, e^{\omega}\, \frac{\omega^{M+1}}{M!}.$$

Finally, Stirling's formula implies $\omega^{M+1}/M!$ decays faster than any power of M^{-1}, so the convergence is super-algebraic and uniform on $[0, 1]$. □

For the monomials $\tau^{p\delta}$, $p = 0, 1, \ldots, n$, we define

$$\phi_p^{(M)}(\tau) := {}^{C}\mathcal{D}^{\delta,\omega}_{\tau,(M)} \tau^{p\delta} = \begin{cases} e^{-\omega\tau} \displaystyle\sum_{k=1}^{M} \frac{\omega^k}{k!} \frac{\Gamma(k + 1)}{\Gamma(k + 1 - \delta)} \tau^{k-\delta}, & p = 0, \\ e^{-\omega\tau} \displaystyle\sum_{k=0}^{M} \frac{\omega^k}{k!} \frac{\Gamma(k + p\delta + 1)}{\Gamma(k + p\delta + 1 - \delta)} \tau^{k+p\delta-\delta}, & p = 1, 2, \ldots, n. \end{cases}$$

For $p = 0$, the term $k = 0$ in the exponential expansion corresponds to a constant, whose classical Caputo derivative is zero. Therefore, in this case the truncated representation starts from $k = 1$.

The truncated derivatives of all monomials $\{\tau^{p\delta}\}_{p=0}^{n}$ define the vector of tempered fractional basis functions:

$$\mathbf{T}_M^*(\tau) = [\phi_0^{(M)}(\tau), \phi_1^{(M)}(\tau), \ldots, \phi_n^{(M)}(\tau)]. \tag{3.13}$$

The vector $\mathbf{T}_M^*(\tau)$ provides a truncated operational representation of the Caputo–tempered derivative based on an analytic series expansion. The independent truncation parameter M enables separation

between truncation and approximation errors, distinguishing the proposed construction from standard operational matrix approaches.

Hence, the tempered fractional derivative of the approximate solution $v_{n,\delta}(\tau) = \mathbf{T}(\tau)\mathbf{Q}^\top\mathbf{C}$ can be written in operational form as

$$ {}^{C}\mathcal{D}_{\tau}^{\delta,\omega} v_{n,\delta}(\tau) \approx \mathbf{T}_M^*(\tau)\,\mathbf{Q}^\top\mathbf{C}. \tag{3.14}$$

The truncation index M controls only the accuracy of the series representation of the tempered operator and is independent of the polynomial degree n. In practice, M is chosen sufficiently large so that the truncation error becomes negligible compared with the discretization error governed by n, ensuring that the overall convergence rate of the method is determined solely by the polynomial approximation.

Substituting (3.9) and (3.14) into (3.1) yields

$$\mathbf{T}_M^*(\tau)\,\mathbf{Q}^\top\mathbf{C} = g(\tau,\, \mathbf{T}(\tau)\mathbf{Q}^\top\mathbf{C})\,, \tag{3.15}$$

which defines the residual

$$\mathcal{R}(\tau;\mathbf{C}) = \mathbf{T}_M^*(\tau)\,\mathbf{Q}^\top\mathbf{C} - g(\tau,\, \mathbf{T}(\tau)\mathbf{Q}^\top\mathbf{C})\,. \tag{3.16}$$

The collocation method enforces the vanishing of this residual at the collocation nodes $\{\tau_j\}_{j=0}^{n-1}$ together with the pointwise condition $v_{n,\delta}(\tau_c) = v_c$, yielding

$$\mathcal{R}(\tau_j;\mathbf{C}) = 0, \quad j = 0, 1, \ldots, n-1, \qquad \mathbf{T}(\tau_c)\mathbf{Q}^\top\mathbf{C} = v_c. \tag{3.17}$$

In vector form, this system can be written as

$$\mathbf{F}(\mathbf{C}) = \mathbf{0}, \tag{3.18}$$

where

$$\mathbf{F}(\mathbf{C}) = [\mathcal{R}(\tau_0;\mathbf{C}), \ldots, \mathcal{R}(\tau_{n-1};\mathbf{C}), \mathbf{T}(\tau_c)\mathbf{Q}^\top\mathbf{C} - v_c]^\top. \tag{3.19}$$

For linear problems $g(\tau, v) = a(\tau)v + f(\tau)$, this reduces to a linear matrix equation $\mathbf{WC} = \mathbf{G}$.

We propose two collocation variants of the TFBM: **TFBM–C**, based on Chebyshev–Gauss nodes, and **TFBM–L**, based on Legendre–Gauss nodes.

The variants TFBM-C and TFBM-L represent two collocation realizations of the same Bernstein–tempered framework, rather than independent numerical methods, and are used to assess the robustness of the formulation under different node distributions.

For **TFBM–C**, the collocation nodes on $[0, 1]$ are defined by

$$\tau_j^{(C)} = \frac{1}{2} + \frac{1}{2}\cos\left(\frac{2j+1}{2n}\pi\right), \qquad j = 0, 1, \ldots, n-1,$$

while for **TFBM–L**, the nodes $\tau_j^{(L)}$, $j = 0, 1, \ldots, n-1$, are given by the roots of the shifted Legendre polynomial $P_n(2\tau - 1)$.

Consequently, the approximate solution $v_{n,\delta}(\tau)$ defined in (3.4) is obtained by solving the system (3.18) for the coefficient vector $\mathbf{C}$ using the Maple software environment. The resulting algebraic system is solved using Maple's `fsolve` command, which automatically selects an appropriate algorithm: A direct solver for linear problems and a Newton-type method for nonlinear systems. In the present implementation, no explicit initial vector is prescribed; the solver is applied directly to the full system, and Maple uses its default internal initialization strategy.

4. Convergence and stability analysis

In this section, we investigate the convergence, error behavior, and stability of the proposed TFBM in the linear setting. The convergence analysis follows the standard framework of spectral and collocation methods, where the error is decomposed into approximation and discrete components; see, e.g., Canuto et al. [42]. We first establish a uniform convergence result for the fractional Bernstein approximation, which provides the theoretical foundation of the method. We then derive an error estimate for the collocation solution based on a decomposition of the approximation and discrete errors. Finally, we examine the stability of the resulting linear system using classical matrix perturbation theory.

4.1. Theoretical convergence

We first recall the uniform approximation property of the fractional Bernstein operator [43].

Theorem 4.1 (Uniform convergence of the fractional Bernstein approximation)**.** *Let $v \in C([0,1])$ and let $0 < \delta < 1$. Define the fractional Bernstein approximation operator by*

$$\widehat{P}_n(v,\tau) := \sum_{\mu=0}^{n} v\left(\left(\frac{\mu}{n}\right)^{1/\delta}\right) \mathcal{B}^{\delta}_{\mu,n}(\tau), \qquad \tau \in [0,1], \tag{4.1}$$

where

$$\mathcal{B}^{\delta}_{\mu,n}(\tau) = \binom{n}{\mu} \tau^{\mu\delta}(1-\tau^{\delta})^{n-\mu}.$$

Then

$$\widehat{P}_n(v,\tau) \longrightarrow v(\tau) \quad \textit{uniformly on } [0,1] \textit{ as } n \to \infty.$$

Proof. Define

$$g(x) := v\left(x^{1/\delta}\right), \qquad x \in [0,1].$$

Since $v \in C([0,1])$ and the mapping $x \mapsto x^{1/\delta}$ is continuous on $[0,1]$, it follows that $g \in C([0,1])$. Hence, g is uniformly continuous on $[0,1]$.

Let $\varepsilon > 0$ be arbitrary. By uniform continuity of g, there exists $\eta > 0$ such that

$$|g(x) - g(y)| < \frac{\varepsilon}{2} \qquad \text{whenever } |x-y| < \eta, \quad x, y \in [0,1]. \tag{4.2}$$

Fix $\tau \in [0,1]$ and set $q := \tau^{\delta} \in [0,1]$. Since $q^{1/\delta} = \tau$, we have $g(q) = v(\tau)$. Define the approximation error

$$\mathcal{E}_n(\tau) := \widehat{P}_n(v,\tau) - v(\tau) = \sum_{\mu=0}^{n} \left(g(\tfrac{\mu}{n}) - g(q)\right) \binom{n}{\mu} q^{\mu}(1-q)^{n-\mu}.$$

Split the index set $\{0, 1, \ldots, n\}$ into

$$\mathcal{I}_{\text{near}}(\tau) := \left\{\mu : \left|\tfrac{\mu}{n} - q\right| < \eta\right\}, \qquad \mathcal{I}_{\text{far}}(\tau) := \left\{\mu : \left|\tfrac{\mu}{n} - q\right| \geq \eta\right\}.$$

If $\mu \in \mathcal{I}_{\text{near}}(\tau)$, then by (4.2) we have $|g(\mu/n) - g(q)| < \varepsilon/2$. Since the Bernstein weights are nonnegative and sum to unity, it follows that

$$\sum_{\mu\in\mathcal{I}_{\text{near}}(\tau)} \left|g(\tfrac{\mu}{n}) - g(q)\right| \binom{n}{\mu} q^{\mu}(1-q)^{n-\mu} \le \frac{\varepsilon}{2}. \tag{4.3}$$

Let

$$K := \max_{x\in[0,1]} |g(x)| = \max_{\tau\in[0,1]} |v(\tau)|.$$

Then, $|g(\mu/n) - g(q)| \le 2K$ for all μ, and hence

$$\sum_{\mu\in\mathcal{I}_{\text{far}}(\tau)} \left|g(\tfrac{\mu}{n}) - g(q)\right| \binom{n}{\mu} q^{\mu}(1-q)^{n-\mu} \le 2K \sum_{\mu\in\mathcal{I}_{\text{far}}(\tau)} \binom{n}{\mu} q^{\mu}(1-q)^{n-\mu}. \tag{4.4}$$

Let $X \sim \text{Bin}(n, q)$. Then, the last sum equals $\mathbb{P}(|X/n - q| \ge \eta)$. By Chebyshev's inequality,

$$\mathbb{P}\Big(\left|\tfrac{X}{n} - q\right| \ge \eta\Big) \le \frac{\text{Var}(X/n)}{\eta^2} = \frac{q(1-q)}{n\eta^2} \le \frac{1}{4n\eta^2},$$

since $q(1-q) \le \frac{1}{4}$ for $q \in [0, 1]$. Substituting into (4.4) yields

$$\sum_{\mu\in\mathcal{I}_{\text{far}}(\tau)} \left|g(\tfrac{\mu}{n}) - g(q)\right| \binom{n}{\mu} q^{\mu}(1-q)^{n-\mu} \le \frac{K}{2n\eta^2}. \tag{4.5}$$

Combining (4.3) and (4.5), we obtain

$$|\mathcal{E}_n(\tau)| \le \frac{\varepsilon}{2} + \frac{K}{2n\eta^2}, \qquad \tau \in [0, 1].$$

Choose $N \in \mathbb{N}$ such that $\frac{K}{2n\eta^2} \le \frac{\varepsilon}{2}$ for all $n \ge N$. Then, $|\mathcal{E}_n(\tau)| \le \varepsilon$ for all $\tau \in [0, 1]$ and all $n \ge N$. Since $\varepsilon > 0$ was arbitrary, the convergence is uniform on $[0, 1]$. □

Remark 4.1. *By setting $g(x) = v(x^{1/\delta})$ and $x = \tau^{\delta}$, the operator $\widehat{P}_n$ can be written as $\widehat{P}_n(v, \tau) = (\mathcal{B}_n g)(x)$, where $\mathcal{B}_n$ denotes the classical Bernstein operator defined in* (2.5)*. Hence, the uniform convergence also follows from the classical Bernstein approximation theorem; see [44].*

Let $x = \tau^{\delta}$. Then,

$$\mathcal{B}^{\delta}_{\mu,n}(\tau) = \binom{n}{\mu} x^{\mu}(1-x)^{n-\mu}, \qquad x = \tau^{\delta}, \tag{4.6}$$

so the fractional Bernstein space

$$\mathcal{V}_n = \text{span}\{\mathcal{B}^{\delta}_{\mu,n}\}_{\mu=0}^{n} \tag{4.7}$$

can be identified with $\mathbb{P}_n$ under the change of variable $x = \tau^{\delta}$. Hence, $\widehat{P}_n(v, \tau)$ is an approximation operator constructed from pointwise samples of the exact solution, whereas $v_{n,\delta}$ is obtained by solving the collocation system.

Since both $\widehat{P}_n(v, \cdot)$ and the collocation solution $v_{n,\delta}$ belong to $\mathcal{V}_n$, we decompose the error as

$$\|v - v_{n,\delta}\|_{\infty} \le \|v - \widehat{P}_n(v, \cdot)\|_{\infty} + \|\widehat{P}_n(v, \cdot) - v_{n,\delta}\|_{\infty}. \tag{4.8}$$

The first term is controlled by Theorem 4.1. We now analyze the second term.

Theorem 4.2 (Convergence of the TFBM collocation solution for the linear case)**.** *Consider the linear TFDE*

$$ {}^{C}\mathcal{D}_{\tau}^{\delta,\omega} v(\tau) = a(\tau)v(\tau) + f(\tau), \qquad v(\tau_c) = v_c, \tag{4.9} $$

where $a, f \in C([0,1])$*, and let* $v \in C([0,1])$ *be the exact solution. Let* $v_{n,\delta} \in \mathcal{V}_n$ *be the TFBM collocation solution obtained from the linear system* $\mathbf{WC}_n = \mathbf{G}$*, and let* $w_n := \widehat{P}_n(v,\cdot) \in \mathcal{V}_n$*.*

Assume that:

(i) (Uniform stability) There exists a constant $K_s > 0$ *such that*

$$ \|\mathbf{W}^{-1}\|_\infty \le K_s \qquad \text{for all } n; $$

(ii) (Discrete consistency) The residual

$$ \mathbf{r}_n := \mathbf{WC}_n^* - \mathbf{G} $$

satisfies

$$ \|\mathbf{r}_n\|_\infty \to 0, \qquad \text{as } n \to \infty, $$

where $\mathbf{C}_n^*$ *denotes the coefficient vector of* w_n*.*

Then,

$$ \|v - v_{n,\delta}\|_\infty \to 0 \qquad \text{as } n \to \infty. $$

Proof. We begin with the error decomposition

$$ \|v - v_{n,\delta}\|_\infty \le \|v - w_n\|_\infty + \|w_n - v_{n,\delta}\|_\infty. \tag{4.10} $$

Since $v_{n,\delta}, w_n \in \mathcal{V}_n$, there exist coefficient vectors $\mathbf{C}_n, \mathbf{C}_n^* \in \mathbb{R}^{n+1}$ such that

$$ v_{n,\delta}(\tau) = \mathbf{T}(\tau)\mathbf{Q}^\top \mathbf{C}_n, \qquad w_n(\tau) = \mathbf{T}(\tau)\mathbf{Q}^\top \mathbf{C}_n^*. $$

From the discrete system,

$$ \mathbf{WC}_n = \mathbf{G}, \qquad \mathbf{WC}_n^* = \mathbf{G} + \mathbf{r}_n, $$

we obtain

$$ \mathbf{C}_n - \mathbf{C}_n^* = -\mathbf{W}^{-1}\mathbf{r}_n, $$

and, hence,

$$ \|\mathbf{C}_n - \mathbf{C}_n^*\|_\infty \le \|\mathbf{W}^{-1}\|_\infty \|\mathbf{r}_n\|_\infty \le K_s \|\mathbf{r}_n\|_\infty. \tag{4.11} $$

To relate the coefficient error to the function error, write

$$ w_n(\tau) - v_{n,\delta}(\tau) = \sum_{\mu=0}^{n} d_\mu \, \mathcal{B}_{\mu,n}^{\delta}(\tau), $$

where d_μ are the components of $\mathbf{C}_n^* - \mathbf{C}_n$. Since the fractional Bernstein basis functions satisfy

$$ \mathcal{B}_{\mu,n}^{\delta}(\tau) \ge 0, \qquad \sum_{\mu=0}^{n} \mathcal{B}_{\mu,n}^{\delta}(\tau) = 1, \qquad \tau \in [0,1], $$

we obtain

$$|w_n(\tau) - v_{n,\delta}(\tau)| \leq \max_{0\leq\mu\leq n} |d_\mu| = \|\mathbf{C}_n - \mathbf{C}_n^*\|_\infty.$$

Hence,

$$\|w_n - v_{n,\delta}\|_\infty \leq \|\mathbf{C}_n - \mathbf{C}_n^*\|_\infty \leq K_s\|\mathbf{r}_n\|_\infty. \tag{4.12}$$

Combining the above estimates yields

$$\|v - v_{n,\delta}\|_\infty \leq \|v - w_n\|_\infty + K_s\|\mathbf{r}_n\|_\infty. \tag{4.13}$$

By Theorem 4.1, we have

$$\|v - w_n\|_\infty \to 0,$$

and by assumption (ii), $\|\mathbf{r}_n\|_\infty \to 0$. Therefore,

$$\|v - v_{n,\delta}\|_\infty \to 0.$$

□

Remark 4.2. *Assumption (i) is a standard stability condition for collocation methods; its validity is supported by the empirical evidence in Section 5 (Tables 3 and 5), where the condition numbers and perturbation ratios remain well controlled.*

Assumption (ii) is motivated by the uniform convergence of the fractional Bernstein approximation (Theorem 4.1) and the super-algebraic decay of the truncation error (Lemma 3.1). These analytical results imply that, for a suitable choice $M = M(n)$, the residual $\|\mathbf{r}_n\|_\infty$ is expected to vanish as $n \to \infty$. This expectation is supported by the numerical experiments: the observed convergence of $v_{n,\delta}$ to v in Tables 2, 4, 7, and 8 is consistent with the decay of $\|\mathbf{r}_n\|_\infty$.

4.2. Numerical error analysis

The accuracy of the proposed TFBM is assessed by comparing the numerical approximation $v_{n,\delta}(\tau)$ with the exact solution at the collocation nodes $\{\tau_j\}_{j=0}^{n-1}$. In particular, we compute the discrete L_∞ error given by

$$\|E_n\|_\infty = \max_{0\leq j\leq n-1} \left|v(\tau_j) - v_{n,\delta}(\tau_j)\right|, \tag{4.14}$$

where $v(\tau)$ denotes the exact solution. The error is evaluated at the interior collocation points to capture the pointwise accuracy of the spectral approximation. This definition is consistent with the approach adopted in Zhao [45], where the discrete maximum norm is used to quantify numerical accuracy in collocation-based methods.

4.3. Stability analysis

TFDEs solved using TFBM require a rigorous stability analysis to ensure the reliability of the numerical solutions. In this context, stability refers to the sensitivity of the discrete TFBM approximation to perturbations arising from the collocation formulation, including variations in the discrete operators and associated data [46, 47]. Two perturbation scenarios are examined, and explicit stability criteria are derived to characterize the robustness of the resulting TFBM collocation matrix systems; see [48, 49].

Applying TFBM to a TFDE yields a discrete collocation matrix system of the form

$$\mathbf{W}\,\mathbf{C} = \mathbf{G}, \tag{4.15}$$

where $\mathbf{W} \in \mathbb{R}^{(n+1)\times(n+1)}$ is the collocation matrix, $\mathbf{C} \in \mathbb{R}^{n+1}$ is the vector of unknown Bernstein coefficients, and $\mathbf{G} \in \mathbb{R}^{n+1}$ is the righthand side vector.

All vector and matrix norms are taken to be the infinity norm $\|\cdot\|_\infty$. Accordingly, for any nonsingular matrix $\mathbf{X}$, we define the corresponding induced condition number by

$$\kappa(\mathbf{X}) := \|\mathbf{X}\|_\infty \, \|\mathbf{X}^{-1}\|_\infty. \tag{4.16}$$

The collocation matrix $\mathbf{W}$ admits the factorization

$$\mathbf{W} = \mathbf{A}\mathbf{Q}^\top, \tag{4.17}$$

where $\mathbf{Q}$ is defined in (3.7) through $\mathbf{B}_n^\delta(\tau) = \mathbf{T}(\tau)\mathbf{Q}^\top$, and $\mathbf{A}$ arises from the collocation equations. For linear problems $g(\tau, v) = a(\tau)v + f(\tau)$,

$$\mathbf{A} = \begin{pmatrix} \mathbf{T}_M^*(\tau_0) - a(\tau_0)\mathbf{T}(\tau_0) \\ \vdots \\ \mathbf{T}_M^*(\tau_{n-1}) - a(\tau_{n-1})\mathbf{T}(\tau_{n-1}) \\ \mathbf{T}(\tau_c) \end{pmatrix}. \tag{4.18}$$

Equivalently, the first n rows of $\mathbf{A}$ are obtained by evaluating the truncated operator

$$\mathcal{L}^{(M)}[\tau^{p\delta}](\tau) := \phi_p^{(M)}(\tau) - a(\tau)\tau^{p\delta}, \qquad p = 0, \ldots, n,$$

at the collocation nodes $\tau_0, \ldots, \tau_{n-1}$, while the last row corresponds to the evaluation of $\tau^{p\delta}$ at τ_c.

The functions $\{\tau^{p\delta}\}_{p=0}^n$ are linearly independent and span the fractional Bernstein approximation space. The invertibility of the associated collocation matrix is therefore linked to the unisolvence of the collocation scheme. We assume that the exact (non-truncated) collocation matrix $\mathbf{A}_*$, obtained by evaluating $\mathcal{L}[\tau^{p\delta}]$ at the collocation nodes, is nonsingular. This is a standard assumption in collocation methods.

By Lemma 3.1, the truncation error satisfies

$$\|\mathbf{A} - \mathbf{A}_*\|_\infty \to 0 \quad \text{as } M \to \infty.$$

Hence, for sufficiently large M, the perturbation satisfies

$$\|\mathbf{A}_*^{-1}(\mathbf{A} - \mathbf{A}_*)\|_\infty < 1,$$

which guarantees that $\mathbf{A}$ remains nonsingular.

Moreover, interpreting $\mathbf{A}$ as a perturbation of $\mathbf{A}_*$,

$$\mathbf{A} = \mathbf{A}_* + (\mathbf{A} - \mathbf{A}_*),$$

the Neumann series argument yields

$$\|\mathbf{A}^{-1}\|_\infty \le \frac{\|\mathbf{A}_*^{-1}\|_\infty}{1 - \|\mathbf{A}_*^{-1}(\mathbf{A} - \mathbf{A}_*)\|_\infty}.$$

Consequently,

$$\kappa(\mathbf{A}) \leq \frac{\|\mathbf{A}\|_\infty \|\mathbf{A}_*^{-1}\|_\infty}{1 - \|\mathbf{A}_*^{-1}(\mathbf{A} - \mathbf{A}_*)\|_\infty}. \tag{4.19}$$

This estimate shows that the conditioning of $\mathbf{A}$ depends on the truncation error of the tempered operator. In particular, as $M \to \infty$, the perturbation $\|\mathbf{A} - \mathbf{A}_*\|_\infty$ decreases, leading to a sharper upper bound on the conditioning of the collocation matrix.

The matrix $\mathbf{Q}$ satisfies $q_{ij} = 0$ for $i > j$ and $q_{ii} = \binom{n}{i} \neq 0$, and is therefore invertible since

$$\det(\mathbf{Q}) = \prod_{i=0}^{n} q_{ii} \neq 0.$$

Consequently, $\mathbf{W} = \mathbf{A}\mathbf{Q}^\top$ is nonsingular for sufficiently large M.

Using the sub-multiplicative property of the induced infinity norm,

$$\kappa(\mathbf{W}) \leq \kappa(\mathbf{A})\, \kappa(\mathbf{Q}^\top). \tag{4.20}$$

Since

$$\|\mathbf{Q}^\top\|_\infty = \|\mathbf{Q}\|_1, \qquad \|(\mathbf{Q}^\top)^{-1}\|_\infty = \|\mathbf{Q}^{-1}\|_1,$$

it follows that

$$\kappa(\mathbf{Q}^\top) = \|\mathbf{Q}\|_1 \|\mathbf{Q}^{-1}\|_1.$$

From the structure of $\mathbf{Q}$ defined in 3.7, we compute the column sums:

$$\sum_{i=0}^{j} |q_{ij}| = \sum_{i=0}^{j} \binom{n}{i}\binom{n-i}{j-i} = \binom{n}{j} 2^j,$$

using a standard combinatorial identity. Hence,

$$\|\mathbf{Q}\|_1 = \max_{0 \leq j \leq n} \binom{n}{j} 2^j.$$

Using the binomial theorem,

$$\binom{n}{j} 2^j \leq \sum_{k=0}^{n} \binom{n}{k} 2^k = (1+2)^n = 3^n,$$

and therefore

$$\|\mathbf{Q}\|_1 \leq 3^n.$$

Moreover,

$$(\mathbf{Q}^{-1})_{ij} = \frac{\binom{j}{i}}{\binom{n}{i}}, \qquad i \leq j,$$

implies

$$\sum_{i=0}^{j} \frac{\binom{j}{i}}{\binom{n}{i}} \leq \sum_{i=0}^{j} 1 = j + 1 \leq n + 1,$$

and, therefore,

$$\|\mathbf{Q}^{-1}\|_1 \leq n + 1.$$

Consequently,

$$\kappa(\mathbf{Q}^\top) \leq (n + 1)3^n, \tag{4.21}$$

Combining (4.19), (4.20), and (4.21), we obtain

$$\kappa(\mathbf{W}) \leq \frac{\|\mathbf{A}\|_\infty \|\mathbf{A}_*^{-1}\|_\infty}{1 - \|\mathbf{A}_*^{-1}(\mathbf{A} - \mathbf{A}_*)\|_\infty} (n + 1)3^n. \tag{4.22}$$

This estimate indicates that the conditioning of $\mathbf{W}$ depends on the conditioning of $\mathbf{A}$ together with the Bernstein transformation matrix $\mathbf{Q}$. The numerical results in Section 5 are consistent with this bound and support the observed stability behavior of the proposed method.

In the numerical stability experiments, perturbations are imposed in a relative, normwise sense. In the implementation, sparse perturbations are employed to control the perturbation magnitude while preserving the structure of the collocation matrix.

Case 1: Perturbations in the righthand side $\mathbf{G}$

Assume $\mathbf{G} \neq \mathbf{0}$ and consider a perturbation $\Delta\mathbf{G}$ in the righthand side:

$$\mathbf{W}(\mathbf{C} + \Delta\mathbf{C}_1) = \mathbf{G} + \Delta\mathbf{G}. \tag{4.23}$$

Subtracting (4.15) yields

$$\mathbf{W}\,\Delta\mathbf{C}_1 = \Delta\mathbf{G} \qquad \Rightarrow \qquad \Delta\mathbf{C}_1 = \mathbf{W}^{-1}\Delta\mathbf{G}. \tag{4.24}$$

Taking norms gives the classical relative perturbation bound

$$\frac{\|\Delta\mathbf{C}_1\|_\infty}{\|\mathbf{C}\|_\infty} \leq \kappa(\mathbf{W}) \frac{\|\Delta\mathbf{G}\|_\infty}{\|\mathbf{G}\|_\infty}. \tag{4.25}$$

To assess (4.25) numerically, we define the normalized ratio

$$r_1 = \frac{\|\Delta\mathbf{C}_1\|_\infty / \|\mathbf{C}\|_\infty}{\kappa(\mathbf{W})\,(\|\Delta\mathbf{G}\|_\infty / \|\mathbf{G}\|_\infty)}. \tag{4.26}$$

Values $r_1 \leq 1$ confirm satisfaction of the theoretical stability bound.

Remark 4.3. *For Case 1, a moderate condition number* $\kappa(\mathbf{W})$ *limits the amplification of righthand side perturbations. Large values of* $\kappa(\mathbf{W})$ *increase sensitivity to data noise and may result in* r_1 *approaching unity, indicating reduced numerical robustness.*

Case 2: Perturbations in both $\mathbf{W}$ *and* $\mathbf{G}$

We now consider simultaneous perturbations in the collocation matrix and righthand side:

$$(\mathbf{W} + \Delta\mathbf{W})(\mathbf{C} + \Delta\mathbf{C}_2) = \mathbf{G} + \Delta\mathbf{G}. \tag{4.27}$$

Neglecting second-order terms yields the first-order approximation

$$\mathbf{W}\,\Delta\mathbf{C}_2 + \Delta\mathbf{W}\,\mathbf{C} \approx \Delta\mathbf{G} \qquad \Rightarrow \qquad \Delta\mathbf{C}_2 \approx \mathbf{W}^{-1}(\Delta\mathbf{G} - \Delta\mathbf{W}\,\mathbf{C}). \tag{4.28}$$

Taking norms gives the bound

$$\frac{\|\Delta\mathbf{C}_2\|_\infty}{\|\mathbf{C}\|_\infty} \le \kappa(\mathbf{W})\left(\frac{\|\Delta\mathbf{G}\|_\infty}{\|\mathbf{G}\|_\infty} + \frac{\|\Delta\mathbf{W}\|_\infty}{\|\mathbf{W}\|_\infty}\right). \tag{4.29}$$

If the Neumann-series condition

$$\|\mathbf{W}^{-1}\Delta\mathbf{W}\|_\infty < 1$$

is satisfied, then $(\mathbf{W} + \Delta\mathbf{W})^{-1}$ exists and the sharper bound

$$\frac{\|\Delta\mathbf{C}_2\|_\infty}{\|\mathbf{C}\|_\infty} \le \frac{\kappa(\mathbf{W})}{1 - \kappa(\mathbf{W})\frac{\|\Delta\mathbf{W}\|_\infty}{\|\mathbf{W}\|_\infty}}\left(\frac{\|\Delta\mathbf{G}\|_\infty}{\|\mathbf{G}\|_\infty} + \frac{\|\Delta\mathbf{W}\|_\infty}{\|\mathbf{W}\|_\infty}\right) \tag{4.30}$$

holds.

We evaluate (4.30) numerically using

$$r_2 = \frac{\|\Delta\mathbf{C}_2\|_\infty/\|\mathbf{C}\|_\infty}{\frac{\kappa(\mathbf{W})}{1 - \kappa(\mathbf{W})\frac{\|\Delta\mathbf{W}\|_\infty}{\|\mathbf{W}\|_\infty}}\left(\frac{\|\Delta\mathbf{G}\|_\infty}{\|\mathbf{G}\|_\infty} + \frac{\|\Delta\mathbf{W}\|_\infty}{\|\mathbf{W}\|_\infty}\right)}. \tag{4.31}$$

Values $r_2 \le 1$ confirm the theoretical perturbation bounds under simultaneous perturbations.

Remark 4.4. *In Case 2, stability critically depends on the condition* $\|\mathbf{W}^{-1}\Delta\mathbf{W}\|_\infty < 1$, *which guarantees bounded invertibility of the perturbed collocation matrix. When satisfied,* $r_2 \le 1$ *indicates that perturbations remain within the theoretical stability limit; values exceeding unity signal potential loss of numerical stability.*

5. Numerical results and discussion

In this section, we present six different test problems to evaluate the proposed TFBM in a comprehensive manner. All examples are defined on an interval $[0, 1]$ with fractional order $0 < \delta < 1$, tempering parameter $\omega \ge 0$, and the truncation index $M = 100$. According to Lemma 3.1, the truncation error decays super-algebraically; for the parameter ranges considered ($\omega \le 3$, $0 < \delta < 1$), the bound becomes negligible already for $M = 100$ (e.g., $\omega^{101}/101!$ is far below machine precision). Tests with $M = 150, 200$ produced identical results, confirming that $M = 100$ is sufficient. These examples assess accuracy on smooth linear TFDEs, robustness under nonlinear dynamics, stability under perturbations, behavior in the presence of weak singularities, and the flexibility of TFBM for multi-order tempered operators. Together, they provide a complete and rigorous validation of the method. All simulations were conducted using Maple 2022 on a system equipped with an Intel Core i7-1260P Central Processing Unit (CPU) (2.10 GHz) and 16 GB RAM, running Windows 11. CPU times were recorded using Maple's `time[real]()` function. All computations were performed with `Digits` = 200 to ensure that the extremely small errors produced at large polynomial degrees are not affected by floating-point round-off limitations.

Example 1. *This example is smooth and linear, and is used to verify the accuracy of the proposed TFBM. We consider the Langevin equation in the form as in [36]*

$$ {}^{C}\mathcal{D}_{\tau}^{\delta,\omega} v(\tau) + v(\tau) = e^{-\omega\tau}\left[\frac{\Gamma(9)}{\Gamma(9-\delta)}\tau^{8-\delta} + \tau^{8} + \tfrac{9}{4}\tau^{\delta} + \tfrac{9}{4}\Gamma(\delta+1)\right], \tag{5.1} $$

with initial condition

$$ v(0) = 0. \tag{5.2} $$

The exact solution is

$$ v(\tau) = e^{-\omega\tau}\left(\tau^{8} + \tfrac{9}{4}\tau^{\delta}\right). \tag{5.3} $$

Example 1 considers a smooth linear tempered fractional problem with an exact solution depending explicitly on the fractional order δ and the tempering parameter ω. As shown in Figure 1, both TFBM-C and TFBM-L produce numerical solutions in close agreement with the exact solution for all tested values of δ using a low polynomial degree $n = 7$, accurately capturing the variation of the solution profile. In particular, as δ increases, the peak magnitude decreases and the solution becomes progressively flatter, especially near the initial region $\tau \approx 0$. This behavior can be attributed to the influence of the fractional order on the regularity of the solution. The numerical curves produced by both methods are visually indistinguishable, not only from each other but also from the exact solution, which indicates a stable and accurate approximation without spurious oscillations. As illustrated in Figure 2, increasing the polynomial degree from $n = 5$ to $n = 11$ leads to a significant reduction in the absolute error. The error is more pronounced near $\tau = 0$ and decreases rapidly as τ increases, in agreement with the fractional nature of the solution. This observation also highlights the capability of the Bernstein basis to approximate smooth functions with high accuracy. The computational cost for Example 1 is summarized in Table 1. For both TFBM-C and TFBM-L, the CPU times remain low and nearly identical for $n = 5$ and $n = 11$, suggesting that increasing the polynomial degree has only a limited effect on the overall computational complexity.

Table 1. CPU time (seconds) for Examples 1–2 with $\delta = \frac{1}{2}$ and $\omega = 3$. Cost increases with n.

	$n = 5$		$n = 11$	
Example	TFBM-C	TFBM-L	TFBM-C	TFBM-L
1	0.63	0.56	0.71	0.70
2	0.87	1.03	2.25	6.20

Example 2. *This example contains a nonlinear term and is used to evaluate the ability of the proposed TFBM to handle nonlinear tempered fractional differential equations [50]. We consider*

$$ {}^{C}\mathcal{D}_{\tau}^{\delta,\omega} v(\tau) = e^{-\omega\tau}\left(\frac{\Gamma(3)}{\Gamma(3-\delta)}\,\tau^{2-\delta} - \left(e^{\omega\tau}v(\tau)\right)^{2} + \tau^{4}\right), \tag{5.4} $$

with initial condition

$$ v(0) = 0. \tag{5.5} $$

The exact solution is

$$ v(\tau) = e^{-\omega\tau}\tau^{2}. \tag{5.6} $$

Example 2 considers a nonlinear tempered fractional problem and therefore provides a more challenging test for the proposed methods. As illustrated in Figure 3, both TFBM-C and TFBM-L accurately approximate the solution, and increasing the polynomial degree from $n = 5$ to $n = 11$ leads to a significant reduction in the absolute error. The error is mainly concentrated near the initial region $\tau \approx 0$. As τ increases, it decreases rapidly and remains small over the rest of the interval. The good performance observed in this nonlinear setting suggests that the collocation formulation remains stable under nonlinear transformations, without introducing additional numerical instability. Both methods exhibit comparable levels of accuracy, with TFBM-C showing slightly lower error in some cases.

The computational cost for Example 2 is reported in Table 1. While both methods require similar CPU time for $n = 5$, a more pronounced increase is observed for TFBM-L at $n = 11$, whereas TFBM-C remains relatively efficient. This difference can be attributed to the increased computational complexity associated with the Legendre-based collocation structure, particularly in the nonlinear setting, which leads to higher evaluation and assembly costs as the polynomial degree increases. Consequently, TFBM-C provides a more favorable balance between accuracy and computational cost for higher polynomial degrees. Overall, these results show that the proposed framework effectively handles nonlinear tempered fractional problems while maintaining both accuracy and computational efficiency.

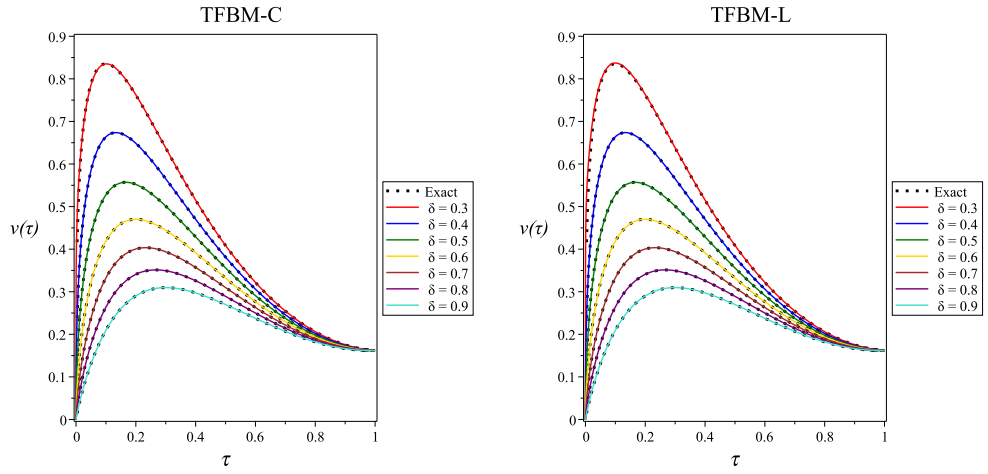

(a) $n = 7, \omega = 3$ (b) $n = 7, \omega = 3$

Figure 1. Exact and numerical solutions obtained using TFBM-C (left panel) and TFBM-L (right panel) for Example 1 with $n = 7$, $\omega = 3$, and $\delta \in \{0.3, \ldots, 0.9\}$. Dots: Exact solution; curves: Numerical approximations for different δ, showing accurate agreement.

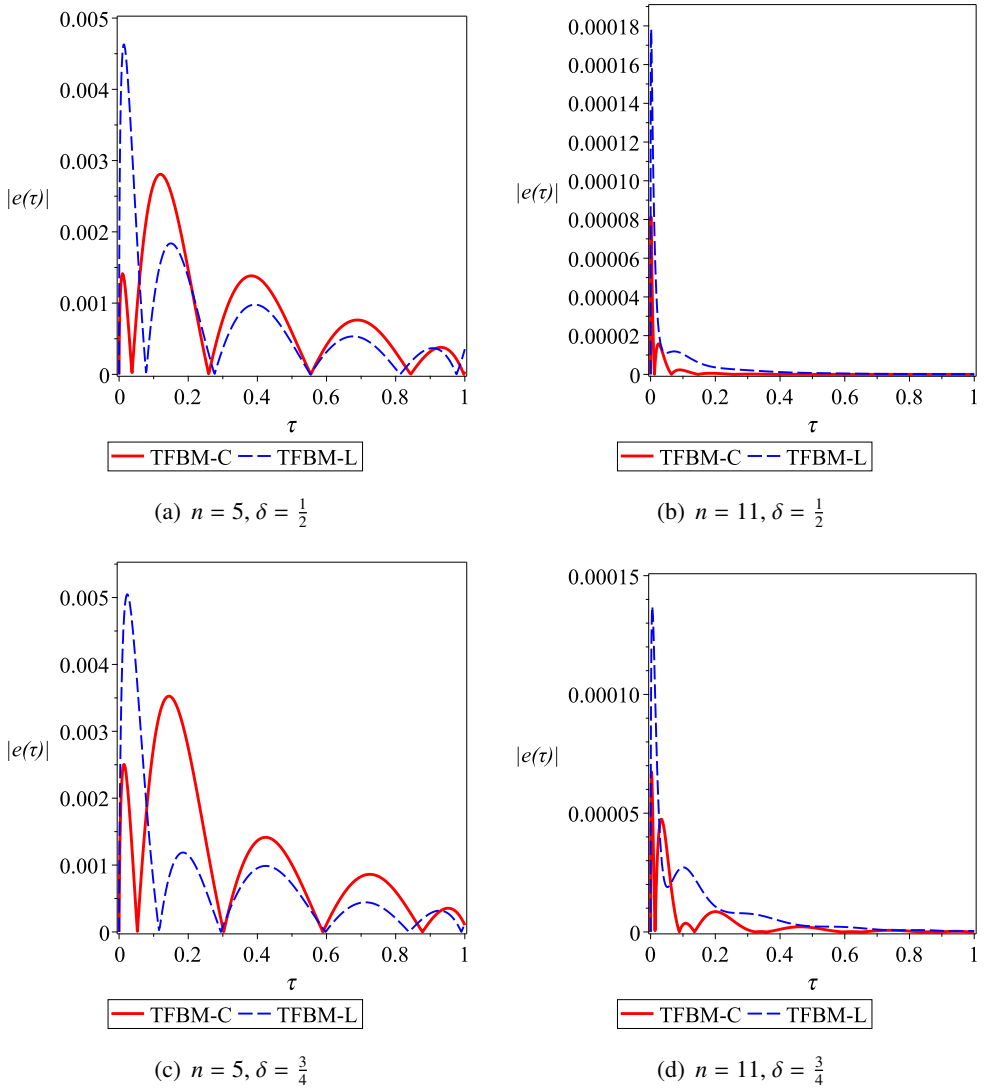

(a) $n = 5, \delta = \frac{1}{2}$ (b) $n = 11, \delta = \frac{1}{2}$

(c) $n = 5, \delta = \frac{3}{4}$ (d) $n = 11, \delta = \frac{3}{4}$

Figure 2. Absolute error $|e(\tau)| = |v(\tau) - v_{n,\delta}(\tau)|$ for Example 1 using TFBM-C and TFBM-L with $\omega = 3$. Panels (a)–(d): $(n, \delta) = (5, \frac{1}{2}), (11, \frac{1}{2}), (5, \frac{3}{4}), (11, \frac{3}{4})$. Error decreases as n increases.

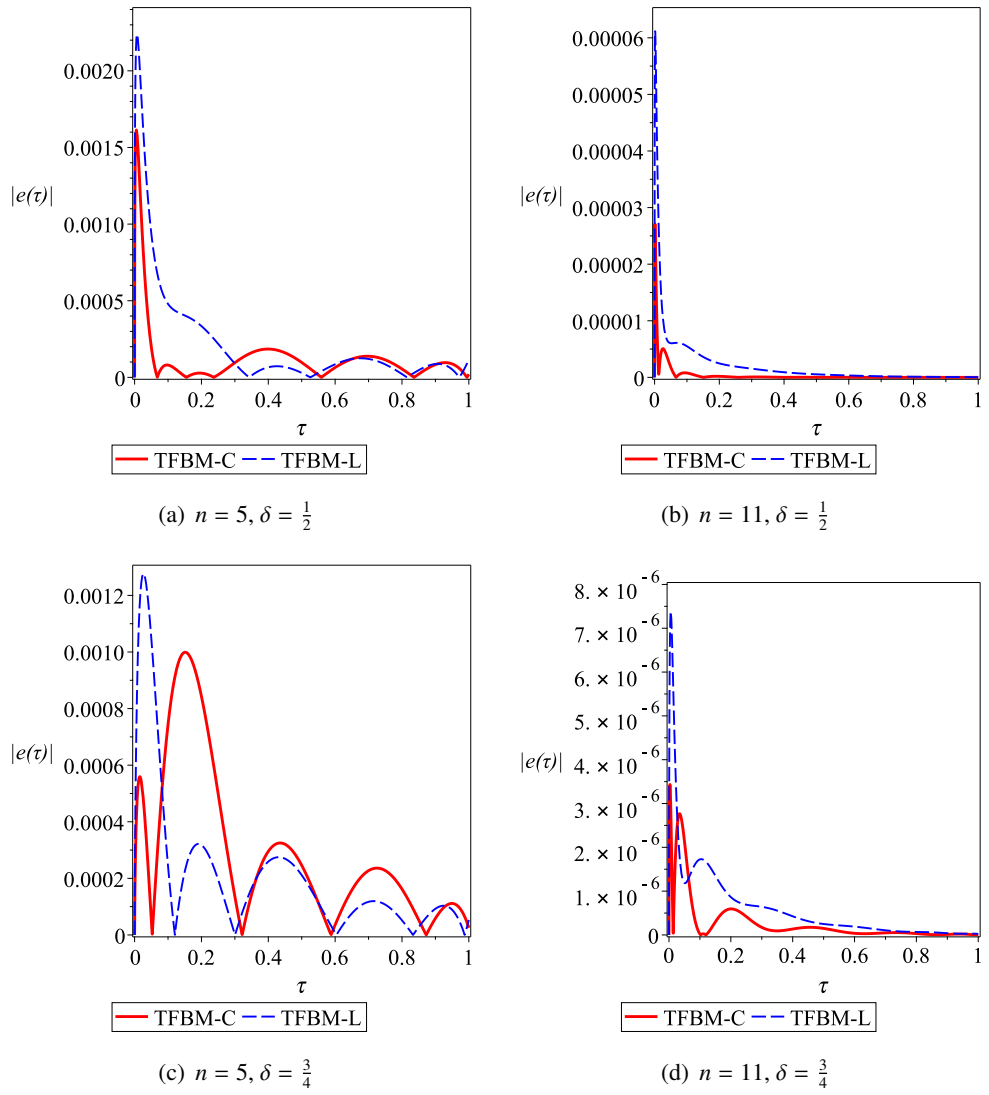

Figure 3. Absolute error $|e(\tau)| = |v(\tau) - v_{n,\delta}(\tau)|$ for Example 2 using TFBM-C and TFBM-L with $\omega = 3$. Panels (a)–(d): $(n, \delta) = (5, \frac{1}{2}), (11, \frac{1}{2}), (5, \frac{3}{4}), (11, \frac{3}{4})$. Error decreases as n increases.

Example 3. *This problem is a standard benchmark from the literature and is used to validate the proposed TFBM through direct comparison with the published results of [51]. We consider*

$$ {}^{C}\mathcal{D}_{\tau}^{\delta,\omega} v(\tau) + c_{\delta,\omega}\, v(\tau) = e^{-\omega\tau}\left[\frac{3\,\Gamma(3)}{4\,\Gamma(3-\delta)}\,\tau^{2-\delta} + \frac{\Gamma(5)}{\Gamma(5-\delta)}\,\tau^{4-\delta} + c_{\delta,\omega}\left(\tau^4 + \tfrac{3}{4}\tau^2\right)\right], \tag{5.7} $$

with the pointwise initial condition

$$ v\left(\tfrac{1}{2}\right) = \frac{e^{-\omega/2}}{4}, \tag{5.8} $$

where

$$ c_{\delta,\omega} = \frac{\Gamma(\delta+1)}{2^{1-\delta}\, e^{\omega/2}}. \tag{5.9} $$

The exact solution is

$$v(\tau) = \left(\tau^4 + \tfrac{3}{4}\tau^2\right) e^{-\omega\tau}. \tag{5.10}$$

Remark. In TFBM, n denotes the polynomial degree, whereas in the reference finite-difference scheme [51], $1/h$ represents the mesh density. Since n and $1/h$ correspond to comparable degrees of freedom in their respective discretizations, matching their values (e.g., $n = 10 \leftrightarrow 1/h = 10$) provides a fair and consistent basis for comparison across the two methods.

Example 3 is a standard benchmark problem from the literature, making it suitable for direct comparison with previously reported results. The results listed in Table 2 confirm that both TFBM-C and TFBM-L achieve significantly lower errors than the reference finite-difference scheme for all tested values of n and for the fractional orders $\delta = \frac{1}{2}$ and $\delta = \frac{2}{3}$. As n increases, the error drops rapidly, and very high accuracy is already obtained for moderate values of n. This behavior is consistent with the expected convergence properties of the proposed methods. A similar trend appears in Figure 4, where the error norms decrease steadily as n increases. Taken together, these observations point to a stable and systematic convergence process. The two methods behave similarly overall, although TFBM-L produces slightly smaller errors in several cases.

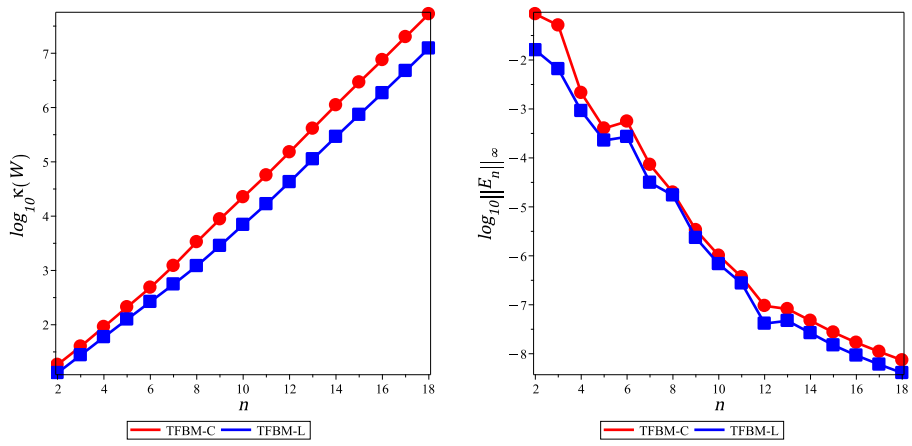

Figure 4. Logarithmic condition number and corresponding error norms for Example 3 with fractional order $\delta = \frac{2}{3}$ and tempering parameter $\omega = 2$. The condition number increases with n, while the error decreases.

Table 2. L_∞ errors for TFBM-C, TFBM-L, and the reference finite-difference scheme for Example 3 with $\delta = \frac{1}{2}, \frac{2}{3}$ and $\omega = 2$. Errors decrease with n, with smaller errors obtained by TFBM-C and TFBM-L.

	$\delta = \frac{1}{2}$			$\delta = \frac{2}{3}$		
n	$\|E_n^{(C)}\|_\infty$	$\|E_n^{(L)}\|_\infty$	$\|E\|_\infty$ [51]	$\|E_n^{(C)}\|_\infty$	$\|E_n^{(L)}\|_\infty$	$\|E\|_\infty$ [51]
10	2.008×10^{-5}	8.992×10^{-6}	5.128×10^{-3}	1.012×10^{-6}	6.800×10^{-7}	9.602×10^{-3}
20	1.435×10^{-10}	9.746×10^{-11}	1.906×10^{-3}	3.522×10^{-9}	1.592×10^{-13}	3.922×10^{-3}
40	1.649×10^{-24}	1.202×10^{-24}	6.978×10^{-4}	3.089×10^{-11}	1.690×10^{-11}	1.587×10^{-3}
80	2.641×10^{-59}	2.361×10^{-59}	2.527×10^{-4}	3.185×10^{-13}	1.716×10^{-13}	6.381×10^{-4}
160	8.577×10^{-132}	1.625×10^{-141}	9.084×10^{-5}	3.650×10^{-15}	1.933×10^{-15}	2.553×10^{-4}

The stability of the proposed schemes is assessed using the logarithmic condition number together with the perturbation ratios shown in Figure 4 and Table 3. The condition number increases moderately with n, and no severe ill-conditioning is observed, so the collocation matrix remains well controlled. The perturbation ratios r_1 and r_2 decrease noticeably as n increases. In practical terms, this corresponds to a lower sensitivity of the numerical solution to perturbations. This reduction in sensitivity supports the robustness of the method and is consistent with the stable structure of the Bernstein-based formulation.

The computational cost for Example 3, reported in Table 6, increases moderately as the polynomial degree grows. For smaller values of n, TFBM-L is slightly more efficient, whereas for larger values, TFBM-C becomes more efficient. In this sense, both methods maintain a good balance between accuracy and computational efficiency across different polynomial degrees.

Overall, the proposed TFBM achieves significantly higher accuracy than the finite-difference scheme, while the computational cost remains moderate. This confirms its effectiveness for benchmark tempered fractional problems.

Table 3. Stability indicators for TFBM–C and TFBM–L for Example 3 ($\delta = \frac{2}{3}$, $\omega = 2$). The logarithmic condition number $\log_{10}\kappa(W)$ and the ratios r_1 and r_2 in (4.26)–(4.31) are reported using relative perturbations $\|\Delta G\|_\infty/\|G\|_\infty = 10^{-4}$ and $\|\Delta W\|_\infty/\|W\|_\infty = 10^{-10}$, showing stable behavior under perturbations.

	TFBM-C			TFBM-L		
n	$\log_{10}\kappa(W)$	r_1	r_2	$\log_{10}\kappa(W)$	r_1	r_2
4	1.96×10^{0}	9.13×10^{-2}	9.13×10^{-2}	1.77×10^{0}	1.37×10^{-1}	1.37×10^{-1}
8	3.52×10^{0}	1.94×10^{-3}	1.94×10^{-3}	3.08×10^{0}	5.33×10^{-3}	5.33×10^{-3}
12	5.18×10^{0}	4.21×10^{-5}	4.21×10^{-5}	4.63×10^{0}	1.49×10^{-4}	1.49×10^{-4}
16	6.87×10^{0}	8.45×10^{-7}	8.37×10^{-7}	6.26×10^{0}	3.43×10^{-6}	3.40×10^{-6}
20	8.57×10^{0}	1.72×10^{-8}	1.58×10^{-8}	7.93×10^{0}	7.47×10^{-8}	6.99×10^{-8}

Example 4. *This example exhibits a weak singularity at $\tau = 0$ and is used to assess the robustness of the proposed TFBM for nonsmooth solutions [51]. We consider*

$$ {}^{C}\mathcal{D}_{\tau}^{\delta,\omega} v(\tau) = e^{-\omega\tau}\,\frac{\Gamma\left(\frac{5}{2}\right)}{\Gamma\left(\frac{5}{2}-\delta\right)}\,\tau^{\frac{3}{2}-\delta}, \qquad 0<\delta<1,\ \omega\geq 0. \tag{5.11} $$

with the pointwise initial condition

$$ v\left(\tfrac{1}{2}\right) = e^{-\omega/2}\sqrt{\tfrac{1}{2^3}}. \tag{5.12} $$

The exact solution is

$$ v(\tau) = e^{-\omega\tau}\,\tau^{3/2}. \tag{5.13} $$

Example 4 considers a test case with a weak singularity at $\tau = 0$, which makes it a challenging setting for the proposed methods. To address this difficulty, the transformation $x = \tau^{\delta}$ is introduced. This transformation regularizes the behavior near the origin and allows the Bernstein approximation to

remain stable. The results in Table 4 confirm that both TFBM-C and TFBM-L achieve high accuracy. As n increases, the error decreases steadily. Near $\tau = 0$, the error is more pronounced, whereas it becomes much smaller away from this region. It is also clear that smaller values of δ lead to stronger singular behavior. For this reason, larger values of n are required to obtain accurate approximations. Figure 5 illustrates the evolution of the condition number and the corresponding error norms with respect to n. Although the condition number increases with n, its growth remains controlled, while the error exhibits a clear decreasing trend. This confirms that the proposed methods maintain high accuracy despite the moderate increase in conditioning. This is consistent with the fractional structure of the solution. Table 5 reports the corresponding stability results. The condition numbers remain moderate as n increases, and no severe ill-conditioning is observed. Overall, the collocation matrix remains well-behaved as n increases. Table 6 shows that the computational cost grows moderately with n. Overall, the results confirm that the proposed methods provide stable and accurate approximations even in the presence of weak singularities.

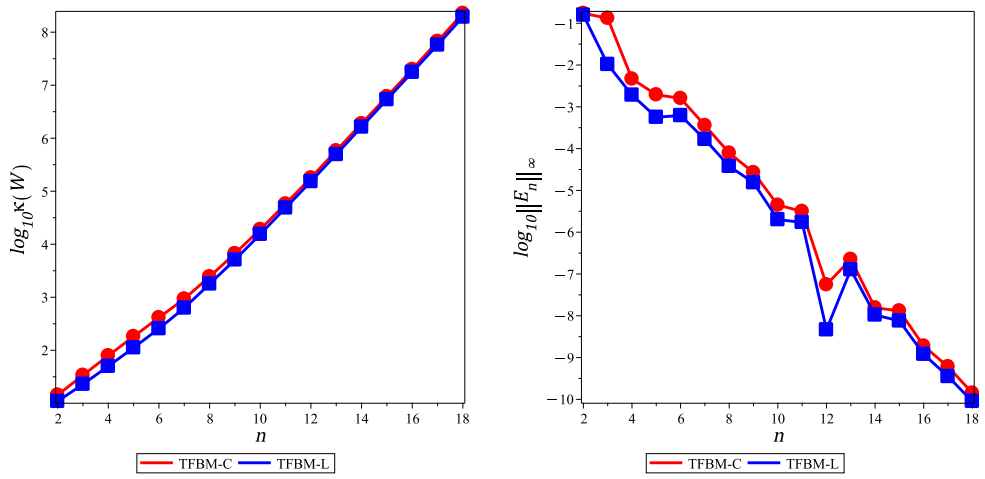

Figure 5. Logarithmic condition number and corresponding error norms for Example 4 with fractional order $\delta = \frac{1}{2}$ and tempering parameter $\omega = 2$. The condition number increases with n, while the error decreases.

Table 4. L_∞ errors for TFBM–C, TFBM–L, and the reference finite-difference scheme for Example 4 with $\delta = \frac{1}{2}$ and $\omega = 2$. Errors decrease with n, with smaller errors obtained by TFBM–C and TFBM–L.

	$\delta = \frac{1}{2}$			
n	$\|\|E_n^{(C)}\|\|_\infty$	$\|\|E_n^{(L)}\|\|_\infty$	$\|\|E\|\|_\infty$ [51]	$\|\|E\|\|_\infty$ [51]
20	8.178×10^{-12}	5.221×10^{-12}	3.304×10^{-3}	7.844×10^{-5}
40	3.246×10^{-27}	2.613×10^{-27}	1.121×10^{-3}	2.955×10^{-5}
80	1.154×10^{-62}	1.083×10^{-62}	4.081×10^{-4}	1.098×10^{-5}
160	2.104×10^{-145}	4.997×10^{-132}	1.472×10^{-4}	3.981×10^{-6}

Table 5. Stability indicators for TFBM–C and TFBM–L for Example 4 ($\delta = \frac{1}{2}$, $\omega = 2$). The logarithmic condition number $\log_{10}\kappa(W)$ and the ratios r_1 and r_2 in (4.26)–(4.31) are reported using relative perturbations $\|\Delta G\|_\infty/\|G\|_\infty = 10^{-4}$ and $\|\Delta W\|_\infty/\|W\|_\infty = 10^{-10}$, showing stable behavior under perturbations.

	TFBM-C			TFBM-L		
n	$\log_{10}\kappa(W)$	r_1	r_2	$\log_{10}\kappa(W)$	r_1	r_2
4	1.90×10^{0}	2.72×10^{-2}	2.72×10^{-2}	1.70×10^{0}	4.34×10^{-2}	4.34×10^{-2}
8	3.39×10^{0}	7.70×10^{-4}	7.70×10^{-4}	3.25×10^{0}	1.06×10^{-3}	1.06×10^{-3}
12	5.25×10^{0}	1.04×10^{-5}	1.04×10^{-5}	5.18×10^{0}	1.23×10^{-5}	1.23×10^{-5}
16	7.30×10^{0}	9.42×10^{-8}	9.31×10^{-8}	7.24×10^{0}	1.07×10^{-7}	1.06×10^{-7}
20	9.40×10^{0}	7.39×10^{-10}	5.99×10^{-10}	9.34×10^{0}	8.55×10^{-10}	7.20×10^{-10}

Table 6. CPU time (seconds) for Examples 3–4 with $\delta = \frac{1}{2}$ and $\omega = 2$. Cost increases with n.

	$n = 20$		$n = 40$		$n = 80$	
Example	TFBM-C	TFBM-L	TFBM-C	TFBM-L	TFBM-C	TFBM-L
3	1.59	1.49	3.53	2.96	15.35	7.61
4	1.81	1.39	3.34	2.70	5.38	11.06

Example 5. *This example involves two tempered fractional derivatives with different tempering parameters and a complex forcing term, demonstrating the generality of the proposed TFBM [27]. We consider*

$$\begin{aligned} {}^{C}\mathcal{D}_{\tau}^{1/2,\,1/2}v(\tau) + {}^{C}\mathcal{D}_{\tau}^{1/2,\,1/4}v(\tau) = \tau^2 v(\tau) - 2\tau^5 - 4\tau^3 \\ + \sqrt{2}\left(\tau^3 + 3\tau^2 - \tau + 5\right)\operatorname{erf}\!\left(\sqrt{\tfrac{\tau}{2}}\right) \\ + \frac{2\tau}{\sqrt{\pi\tau}}\,e^{-\tau/2}\left(\tau^2 + 2\tau - 1\right) \\ + \left(\tau^3 + 6\tau^2 - 10\tau + 28\right)\operatorname{erf}\!\left(\tfrac{\sqrt{\tau}}{2}\right) \\ + \frac{2\tau}{\sqrt{\pi\tau}}\,e^{-\tau/4}\left(\tau^2 + 4\tau - 10\right). \end{aligned} \tag{5.14}$$

with initial condition

$$v(0) = 0. \tag{5.15}$$

The exact solution is

$$v(\tau) = 2\tau^3 + 4\tau. \tag{5.16}$$

Example 6. *This example involves two different fractional orders with the same tempering parameter and is used to examine the effect of varying the fractional order δ within the proposed TFBM framework [27]. We consider*

$${}^{C}\mathcal{D}_{\tau}^{1/2,\,1/2}v(\tau) + {}^{C}\mathcal{D}_{\tau}^{1/4,\,1/2}v(\tau) = \frac{16\,e^{-\tau/2}\,\tau^{3/2}}{3\,\sqrt{\pi}} + \frac{64\,e^{-\tau/2}\,\tau^{7/4}}{21\,\sqrt{3/4}}, \tag{5.17}$$

with initial condition

$$v(0) = 0. \tag{5.18}$$

The exact solution is

$$v(\tau) = 2\, e^{-\tau/2}\, \tau^2. \tag{5.19}$$

Examples 5 and 6 further assess the performance of the proposed TFBM for multi-term tempered fractional differential equations. The absolute and relative errors reported in Tables 7 and 8 show that both TFBM-C and TFBM-L consistently outperform the shifted Legendre operational matrix method [27], often by several orders of magnitude. In Example 5, the presence of multiple tempered fractional derivatives with distinct tempering parameters increases the complexity of the operator representation.The results show that the proposed Bernstein-based formulation is able to handle this multi-term structure effectively, without any loss of accuracy. In Example 6, comparable accuracy is obtained for different values of the fractional order δ. This indicates that the method remains stable even when the fractional dynamics vary.

Table 7. Absolute errors for Example 5 at $n = 6$, showing smaller errors for TFBM-C and TFBM-L compared to the Shifted Legendre operational matrix method.

τ	TFBM-C	TFBM-L	Shifted Legendre [27]
0.1	2.07956×10^{-191}	3.61530×10^{-193}	2.72390×10^{-3}
0.2	2.68705×10^{-192}	1.12219×10^{-192}	6.74832×10^{-3}
0.3	5.92059×10^{-192}	2.24328×10^{-192}	6.06411×10^{-3}
0.4	1.47550×10^{-192}	1.57507×10^{-192}	1.63810×10^{-3}
0.5	5.25594×10^{-192}	5.04773×10^{-193}	2.20223×10^{-3}
0.6	6.31429×10^{-192}	2.94071×10^{-193}	1.38416×10^{-3}
0.7	6.02368×10^{-193}	1.10036×10^{-192}	4.29494×10^{-3}
0.8	5.34968×10^{-192}	1.72823×10^{-192}	7.55232×10^{-3}
0.9	2.39609×10^{-192}	3.83042×10^{-193}	9.99599×10^{-3}
1.0	4.46720×10^{-191}	9.09196×10^{-192}	8.14496×10^{-2}

Table 8. Relative absolute errors for Example 6 at $n = 8$ and $n = 10$, showing smaller errors for TFBM-C and TFBM-L compared to the Shifted Legendre operational matrix method.

	$n = 8$			$n = 10$		
τ	TFBM-C	TFBM-L	[27]	TFBM-C	TFBM-L	[27]
0.2	1.48×10^{-198}	1.36×10^{-198}	9.61×10^{-4}	1.33×10^{-197}	3.32×10^{-196}	2.42×10^{-4}
0.4	6.88×10^{-199}	9.38×10^{-200}	6.15×10^{-5}	2.38×10^{-198}	6.07×10^{-197}	9.18×10^{-6}
0.6	3.06×10^{-199}	4.31×10^{-199}	4.81×10^{-5}	2.07×10^{-198}	2.24×10^{-197}	2.89×10^{-5}
0.8	7.81×10^{-199}	6.25×10^{-199}	7.27×10^{-5}	3.98×10^{-198}	1.09×10^{-197}	2.39×10^{-6}

The numerical results are in agreement with the theoretical analysis presented in Section 4. As the polynomial degree increases, a systematic reduction in the error is observed. The transformation

$x = \tau^{\delta}$ plays an important role in capturing fractional-type behavior near $\tau = 0$. At the same time, the Bernstein basis contributes to a stable and well-conditioned approximation framework across different parameter regimes.

6. Conclusions

In this work, a TFBM has been developed for the numerical solution of tempered fractional differential equations with Caputo-type derivatives. Two collocation-based variants, namely, TFBM-C and TFBM-L, were constructed within a unified Bernstein operational matrix framework and applied to a wide range of problems, including linear and nonlinear equations, multi-term models, and problems with weakly singular solutions.

A convergence analysis was carried out. The uniform convergence of the fractional Bernstein approximation provides the approximation foundation of the method. In addition, the truncation error associated with the tempered Caputo derivative was shown to decay super-algebraically, ensuring that the operator approximation does not limit the overall accuracy. For linear TFDEs, convergence of the collocation solution was established under two standard assumptions: Uniform stability of the collocation matrices and discrete consistency of the scheme. These assumptions are standard in spectral collocation methods; the former is supported numerically, while the latter follows from the truncation estimate together with the approximation properties of the Bernstein basis. The analysis provides a clear theoretical explanation for the numerical accuracy observed in the computational experiments.

The stability of the proposed approach was investigated through a perturbation-based analysis, which confirmed the robustness of the resulting linear systems. In particular, the numerical stability indicators were shown to remain within the derived bounds even as the condition numbers increased.

Extensive numerical experiments further demonstrated that the proposed method achieves substantially higher accuracy than existing operational matrix and finite-difference schemes for the problems considered, while maintaining reasonable computational efficiency. Taken together, these results indicate that TFBM offers a reliable, well-conditioned, and flexible framework for tempered fractional modeling. The proposed methodology also naturally lends itself to further extensions, including tempered integro-differential equations, nonlinear tempered systems, and tempered fractional partial differential equations, as well as applications to tempered fractional epidemic models.

Author contributions

J. Al Hallak: Conceptualization, methodology, software, data curation, visualization, writing – original draft, funding acquisition; J. Al Hallak and I. Hashim: Formal analysis; J. Al Hallak, M. Alshbool and I. Hashim: Investigation; J. Al Hallak, M. Alshbool, I. Hashim, E. S. Ismail and S. Momani: Validation, writing – review & editing; M. Alshbool, I. Hashim and E. S. Ismail: Supervision, project administration. All authors have read and approved the final version of the manuscript for publication.

Use of Generative-AI tools declaration

The authors declare that no generative Artificial Intelligence (AI) tools were used in the creation of this article.

Conflict of interest

The authors declare that there is no conflict of interest.

References

1. A. Bibi, M. ur Rehman, A numerical method for solutions of tempered fractional differential equations, *J. Comput. Appl. Math.,* **443** (2024), 115772. http://dx.doi.org/10.1016/j.cam.2024.115772
2. M. D. Johansyah, A. K. Supriatna, E. Rusyaman, J. Saputra, Application of fractional differential equation in economic growth model: A systematic review approach, *AIMS Math.,* **6** (2021), 10266–10280. http://dx.doi.org/10.3934/math.2021594
3. J. L. Suzuki, M. Gulian, M. Zayernouri, M. D'Elia, Fractional modeling in action: A survey of nonlocal models for subsurface transport, turbulent flows, and anomalous materials, *J. Peridynam. Nonlocal Model.,* **5** (2023), 392–459. http://dx.doi.org/10.1007/s42102-022-00085-2
4. J. Al Hallak, M. Alshbool, I. Hashim, Implementing Bernstein operational matrices to solve a fractional-order smoking epidemic model, *Int. J. Differ. Equ.,* **2024** (2024), 9141971. http://dx.doi.org/10.1155/2024/9141971
5. J. Al Hallak, M. H. T. Alshbool, I. Hashim, Numerical solution of a fractional SEIR epidemic model using Bernstein series approximation method, *AIP Confer. Proc.,* **3338** (2025), 040011. http://dx.doi.org/10.1063/5.0295817
6. M. Borah, A. Gayan, J. S. Sharma, Y. Chen, Z. Wei, V. T. Pham, Is fractional-order chaos theory the new tool to model chaotic pandemics as Covid-19?, *Nonlinear Dynam.,* **109** (2022), 1187–1215. http://dx.doi.org/10.1007/s11071-021-07196-3
7. T. Eriqat, R. Saadeh, A. El-Ajou, A. Qazza, M. A. N. Oqielat, A. Ghazal, A new analytical algorithm for uncertain fractional differential equations in the fuzzy conformable sense, *AIMS Math.,* **9** (2024), 9641–9681. http://dx.doi.org/10.3934/math.2024472
8. C. Coelho, M. F. P. Costa, L. L. Ferrás, Neural fractional differential equations, *Appl. Math. Model.,* **144** (2025), 116060. http://dx.doi.org/10.1016/j.apm.2025.116060
9. M. M. Raja, V. Vijayakumar, K. C. Veluvolu, Higher-order Caputo fractional integrodifferential inclusions of Volterra–Fredholm type with impulses and infinite delay: Existence results, *J. Appl. Math. Comput.,* **71** (2025), 4849–4874. http://dx.doi.org/10.1007/s12190-025-02412-4
10. M. Raja, V. Vijayakumar, K. C. Veluvolu, An analysis on approximate controllability results for impulsive fractional differential equations of order $1 < r < 2$ with infinite delay using sequence method, *Math. Method. Appl. Sci.,* **47** (2024), 336–351. http://dx.doi.org/10.1002/mma.9657

11. F. Sabzikar, M. M. Meerschaert, J. Chen, Tempered fractional calculus, *J. Comput. Phys.,* **293** (2015), 14–28. http://dx.doi.org/10.1016/j.jcp.2014.04.024
12. S. Chen, J. Shen, L. L. Wang, Laguerre functions and their applications to tempered fractional differential equations on infinite intervals, *J. Sci. Comput.,* **74** (2018), 1286–1313. http://dx.doi.org/10.1007/s10915-017-0495-7
13. W. Deng, Z. Zhang, Variational formulation and efficient implementation for solving the tempered fractional problems, *Numer. Method. Part. Diff. Equ.,* **34** (2018), 1224–1257. http://dx.doi.org/10.1002/num.22254
14. A. El-Abed, S. A. Dahy, H. M. El-Hawary, T. Aboelenen, A. Fahim, High-order Chebyshev pseudospectral tempered fractional operational matrices and tempered fractional differential problems, *Fractal Fract.,* **7** (2023), 777. http://dx.doi.org/10.3390/fractalfract7110777
15. B. Shiri, G. C. Wu, D. Baleanu, Collocation methods for terminal value problems of tempered fractional differential equations, *Appl. Numer. Math.,* **156** (2020), 385–395. http://dx.doi.org/10.1016/j.apnum.2020.05.007
16. M. A. Zaky, Existence, uniqueness and numerical analysis of solutions of tempered fractional boundary value problems, *Appl. Numer. Math.,* **145** (2019), 429–457. http://dx.doi.org/10.1016/j.apnum.2019.05.008
17. R. Almeida, N. Martins, J. V. da C. Sousa, Fractional tempered differential equations depending on arbitrary kernels, *AIMS Math.,* **9** (2024), 9107–9127. http://dx.doi.org/10.3934/math.2024443
18. A. Liemert, A. Kienle, Fundamental solution of the tempered fractional diffusion equation, *J. Math. Phys.,* **56** (2015), 113301. http://dx.doi.org/10.1063/1.4935475
19. J. Li, Z. Qiu, Fourth-order effective approximation of the normalized Riemann–Liouville tempered fractional derivatives and its applications, *AIMS Math.,* **10** (2025), 17801–17831. http://dx.doi.org/10.3934/math.2025794
20. Z. Qiu, Fourth-order high-precision algorithms for one-sided tempered fractional diffusion equations, *AIMS Math.,* **9** (2024), 27102–27121. http://dx.doi.org/10.3934/math.20241318
21. H. K. Dwivedi, A novel fast second order approach with high-order compact difference scheme and its analysis for the tempered fractional Burgers equation, *Math. Comput. Simulat.,* **227** (2025), 168–188. http://dx.doi.org/10.1016/j.matcom.2024.08.003
22. H. Zhang, M. Liu, T. Guo, D. Xu, Three finite difference schemes for generalized nonlinear integro-differential equations with tempered singular kernel, *Math. Comput. Simulat.,* **225** (2024), 1199–1217. http://dx.doi.org/10.1016/j.matcom.2024.01.026
23. C. Li, W. Deng, High order schemes for the tempered fractional diffusion equations, *Adv. Comput. Math.,* **42** (2016), 543–572. http://dx.doi.org/10.1007/s10444-015-9434-z
24. C. Li, W. Deng, L. Zhao, Well-posedness and numerical algorithm for the tempered fractional differential equations, *Discrete Contin. Dynam. Syst.-B,* **24** (2019), 1989–2015. http://dx.doi.org/10.3934/dcdsb.2019026
25. J. Deng, L. Zhao, Y. Wu, Fast predictor–corrector approach for the tempered fractional differential equations, *Numer. Algorithms,* **74** (2017), 717–754. http://dx.doi.org/10.1007/s11075-016-0169-9

26. B. P. Moghaddam, J. A. T. Machado, A. Babaei, A computationally efficient method for tempered fractional differential equations with application, *Comput. Appl. Math.,* **37** (2018), 3657–3671. http://dx.doi.org/10.1007/s40314-017-0522-1

27. A. E. Owoyemi, C. Phang, Y. T. Toh, An efficient numerical scheme for solving multiorder tempered fractional differential equations via operational matrix, *J. Math.,* **2022** (2022), 7628592. http://dx.doi.org/10.1155/2022/7628592

28. N. A. Obeidat, D. E. Bentil, Novel technique to investigate the convergence analysis of the tempered fractional natural transform method applied to diffusion equations, *J. Ocean Eng. Sci.,* **8** (2023), 636–646. http://dx.doi.org/10.1016/j.joes.2022.05.014

29. S. Saifullah, A. Ali, A. Khan, K. Shah, T. Abdeljawad, A novel tempered fractional transform: theory, properties and applications to differential equations, *Fractals,* **31** (2023), 2340045. http://dx.doi.org/10.1142/S0218348X23400455

30. L. Zhao, W. Deng, J. S. Hesthaven, Spectral methods for tempered fractional differential equations, *Math. Comput.,* **85** (2016), 283–318.

31. L. Mansouri, Z. Azimzadeh, Numerical solution of fractional delay Volterra integro-differential equations by Bernstein polynomials, *Math. Sci.,* **17** (2023), 455–466. https://doi.org/10.1007/s40096-022-00463-3

32. N. Mohamed, M. A. Eltaher, S. A. Mohamed, E. Carrera, Bernstein polynomials in analyzing nonlinear forced vibration of curved fractional viscoelastic beam with viscoelastic boundaries, *Acta Mech.,* **235** (2024), 4541–4561. https://doi.org/10.1007/s00707-024-03954-7

33. L. S. Salih, S. S. Ahmed, A Bernstein operational matrix approach for solving certain nonlinear Volterra–Fredholm integro-differential equations involved by Caputo fractional derivative, *J. Univ. Babylon Pure Appl. Sci.,* **33** (2025), 309–354. https://doi.org/10.29196/jubpas.v33i3.6013

34. Z. Hu, K. Kawaguchi, Z. Zhang, G. E. Karniadakis, Tackling the curse of dimensionality in fractional and tempered fractional PDEs with physics-informed neural networks, *Comput. Method. Appl. M.,* **432** (2024), 117448. http://dx.doi.org/10.1016/j.cma.2024.117448

35. M. Medveď, E. Brestovanská, Differential equations with tempered ψ-Caputo fractional derivative, *Math. Model. Anal.,* **26** (2021), 631–650. http://dx.doi.org/10.3846/mma.2021.13252

36. N. A. Obeidat, D. E. Bentil, New theories and applications of tempered fractional differential equations, *Nonlinear Dynam.,* **105** (2021), 1689–1702. http://dx.doi.org/10.1007/s11071-021-06628-4

37. M. H. T. Alshbool, M. Mohammad, O. Isik, I. Hashim, Fractional Bernstein operational matrices for solving integro-differential equations involved by Caputo fractional derivative, *Results Appl. Math.,* **14** (2022), 100258. http://dx.doi.org/10.1016/j.rinam.2022.100258

38. M. H. T. Alshbool, Bernstein polynomials method for solving multi-order fractional neutral pantograph equations with error and stability analysis, *Results Appl. Math.,* **22** (2024), 100451. http://dx.doi.org/10.1016/j.rinam.2024.100451

39. N. I. N. Kamarul Bahrim, M. Y. Misro, Solving the Lane–Emden equation by using Bernstein operational matrix, *Alex. Eng. J.,* **129** (2025), 278–288. http://dx.doi.org/10.1016/j.aej.2025.06.001

40. W. Gautschi, Some elementary inequalities relating to the gamma and incomplete gamma function, *J. Math. Phys.,* **38** (1959), 77–81.

41. M. Abramowitz, I. A. Stegun, *Handbook of mathematical functions*, Dover, New York, 1965.

42. C. Canuto, M. Y. Hussaini, A. Quarteroni, T. A. Zang, *Spectral methods: Fundamentals in single domains*, Springer, 2007.

43. N. Sriwastav, A. K. Barnwal, A. M. Wazwaz, M. Singh, Bernstein operational matrix of differentiation and collocation approach for a class of three-point singular BVPs: Error estimate and convergence analysis, *Opusc. Math.,* **43** (2023), 575–601. http://dx.doi.org/10.7494/OpMath.2023.43.4.575

44. G. G. Lorentz, *Bernstein polynomials*, American Mathematical Society, Providence, RI, 2012.

45. T. Zhao, Efficient spectral collocation method for tempered fractional differential equations, *Fractal Fract.,* **7** (2023), 277. http://dx.doi.org/10.3390/fractalfract7030277

46. N. J. Higham, *Accuracy and stability of numerical algorithms*, SIAM, Philadelphia, 2002. http://dx.doi.org/10.1137/1.9780898718027

47. G. H. Golub, C. F. Van Loan, *Matrix computations*, 4 Eds., Johns Hopkins University Press, Baltimore, 2013.

48. G. W. Stewart, *Perturbation theory for the singular value decomposition*, Technical Report CS-TR-2539, University of Maryland, 1990.

49. M. Khuddush, K. R. Prasad, Existence, uniqueness and stability analysis of a tempered fractional order thermistor boundary value problems, *J. Anal.,* **31** (2023), 85–107. http://dx.doi.org/10.1007/s41478-022-00438-6

50. M. S. Heris, M. Javidi, A predictor–corrector scheme for the tempered fractional differential equations with uniform and non-uniform meshes, *J. Supercomput.,* **75** (2019), 8168–8206. http://dx.doi.org/10.1007/s11227-019-02979-3

51. M. L. Morgado, M. Rebelo, Well-posedness and numerical approximation of tempered fractional terminal value problems, *Fract. Calc. Appl. Anal.,* **20** (2017), 1239–1262. http://dx.doi.org/10.1515/fca-2017-0065

AIMS Press